Synergistic Experimental and Computational Approach Identifies Novel Strategies for PHB Overproduction

Adil Alsiyabi
University of Nebraska-Lincoln
Brandi Brown
University of Nebraska-Lincoln
Cheryl Immethun
University of Nebraska-Lincoln
Mark Wilkins
University of Nebraska-Lincoln
Rajib Saha (rsaha2@unl.edu)
University of Nebraska-Lincoln https://orcid.org/0000-0002-2974-0243

Article

Keywords: Polyhydroxyalkanoates, Lignin, Metabolic modeling, Bioplastics

Posted Date: March 17th, 2021

DOI: https://doi.org/10.21203/rs.3.rs-334477/v1

Synergistic Experimental and Computational Approach Identifies Novel Strategies for PHB Overproduction

Adil Alsiyabi[a,*], Brandi Brown[b,*], Cheryl Immethun[a], Mark Wilkins[b,c,d] & Rajib Saha[a]

[a] *Department of Chemical and Biomolecular Engineering, University of Nebraska-Lincoln, Lincoln, NE 68588, USA*

** First author. These authors contributed equally to this work*

[b] *Department of Biological Systems Engineering, University of Nebraska-Lincoln, Lincoln, NE 68583, USA*

[c] *Industrial Agricultural Products Center, University of Nebraska-Lincoln, Lincoln, NE 68583, USA*

[d] *Department of Food Science and Technology, University of Nebraska-Lincoln, Lincoln, NE 68588, USA*

Keywords: Polyhydroxyalkanoates, Lignin, Metabolic modeling, Bioplastics

Abstract

Polyhydroxybutyrate (PHB) is a sustainable bioplastic produced by bacteria that is a potential replacement for conventional plastics. This study delivers an integrated experimental and computational modeling approach to decipher metabolic factors controlling PHB production and offers engineering design strategies to boost production. In the metabolically robust *Rhodopseudomonas palustris* CGA009, PHB production significantly increased when grown on the carbon- and electron-rich lignin breakdown product *p*-coumarate ($C_9H_8O_3$) compared to acetate when the same amount of carbon was supplied. However, the maximum yield did not improve further when grown on coniferyl alcohol ($C_{10}H_{12}O_3$). In order to obtain a systems-level understanding of factors driving PHB yield, a model-driven investigation was performed. The model yielded several engineering design strategies including utilizing reduced, high molecular weight substrates that bypass the thiolase reaction. Overall, these findings uncover key parameters controlling PHB production and design strategies that can potentially be expanded to any bacterium for optimizing PHB production.

Introduction

Due to the global plastic waste crisis, there has been extensive research on polyhydroxyalkanoates (PHAs) as potential replacements for petroleum-derived plastics. PHAs are biopolymers produced by bacteria that have similar thermomechanical properties as conventional plastics, but are also biodegradable, have shown biocompatibility in therapeutics, and can be produced from a wide array of sustainable carbon sources[1,2]. These bioplastics are generally produced by microbes under stressful conditions (e.g. nutrient starvation) and stored as granules inside the cytoplasm for carbon balance, stress mitigation, and as a redox sink[3]. PHAs are considered to be the largest group of natural polyesters with over 150 monomers reported and offer a unique platform for easily manipulating the thermomechanical properties of the bioplastic produced[4]. Due to these characteristics, PHAs have been used in a wide array of applications ranging from medical implants to biodegradable packaging[2,5,6]. However, the widespread adoption of PHAs is hampered by high production costs, which is largely attributed to feedstock costs[7]. Therefore, engineering a microbe that can overproduce the most common form of PHA, called polyhydroxybutyrate (PHB), from inexpensive renewable feedstocks is needed.

However, choosing the right engineering strategy to maximize PHB production can be tricky due to the complexity in metabolism across PHB-producing bacteria[8]. PHB synthesis has been investigated extensively in multiple organisms[5,9–16] but different studies primarily point to three different bottlenecks that constrict the rate through the pathway[9–16]. First, a number of studies have indicated that the rate of PHB synthesis is dependent on the acetyl-CoA pool size or the acetyl-CoA/CoA ratio[13,14]. Since acetyl-CoA is the first substrate in the pathway, it is intuitive to postulate that increasing its intracellular concentration will lead to an increase in the rate of PHB synthesis. Indeed, this has been shown in *Saccharomyces cerevisiae*[14]. Furthermore, the first reaction in the PHB pathway (thiolase) is thermodynamically unfavorable in the forward direction ($\Delta G'° = 26\ kJ/mol$), which means that the ratio of reactants to products should be high in order for this reaction to proceed. This hypothesis is related to the pathway's role as a carbon sink, as any increase in the production of the central metabolite (i.e., acetate) will be funneled towards PHB for storage[17]. Second, other studies have reported that the rate of PHB synthesis is correlated to the redox state of NADPH ([NADPH]/[NADP])[18–21]. This observation can be connected to the pathway's role as an electron sink[17]. Furthermore, an increase in the NADPH to NADP ratio increases the thermodynamic driving force of the second reaction in the pathway (reductase). Third, a study investigating the effect of overexpressing different enzymes in the pathway found that the expression of the reductase was the limiting factor in PHB synthesis[12]. This result is consistent with a number of previous kinetic analyses which revealed that the catalytic efficiency of the reductase reaction was substantially lower than that of other reactions in the pathway[22,23]. Interestingly, this study also shows that an increase in the expression of the thiolase actually leads to a slight decrease in PHB production, which further points to the thermodynamic driving force favoring the reverse direction of the reaction[12].

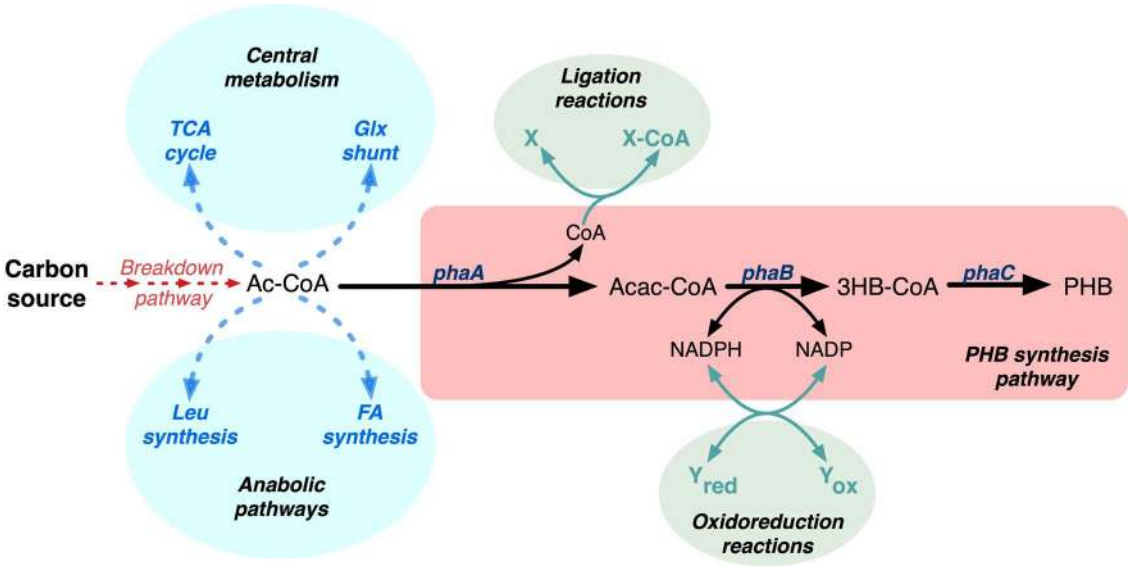

Fig. 1: PHB synthesis in the context of whole-cell metabolism.

Based on these findings, it is apparent that the activity of the pathway is highly dependent on metabolic factors such as the relative abundance of the participating metabolites and cofactors. Furthermore, due to the inherently high connectivity of the participating metabolites, their condition-specific availability is reliant on their overall generation and consumption rates from a number of different pathways. It is therefore vital to make use of a systems-wide framework such as genome-scale metabolic models (GSMMs) that can account for changes that occur in all parts of the metabolic network. These models translate the repertoire of all known metabolic functionalities performed by an organism into a mathematical representation which can then be used to predict the activity throughout the metabolic network[24–26]. With the aid of methods such as Flux Balance Analysis (FBA)[27], GSMMs have been successful in accurately predicting how metabolism changes under different genetic and environmental perturbations, as well as generating testable hypotheses on what drives such changes. Thus far, GSMMs of several PHB producing bacteria have been reconstructed[12,28–31]. These models were mainly used to explain observed behavior (e.g., storage metabolism under feast-famine cycles) in the specific organism of interest and accordingly only considered a subset of the possible metabolic states. Therefore, a holistic understanding of how the PHB pathway interacts with the rest of the metabolic network is crucial for obtaining a set of generalized design strategies to increase PHB productivity.

The metabolically diverse *Rhodopseudomonas palustris* CGA009 (hereafter *R. palustris*) is an ideal candidate for deciphering key engineering design strategies for PHB production using a GSMM. *R. palustris* can utilize a wide variety of carbon sources in both aerobic and anerobic conditions, including over two dozen aromatic compounds from lignin[32,33], an underutilized abundant raw material that would be toxic to many microbes used in industrial bioprocessing. Of note, *R.*

palustris is renowned for its metabolism of the lignin breakdown product (LBP) *p*-coumarate, as well as its ability to perform anoxic photosynthesis and fix CO_2[34].

In this study, *R. palustris* was grown on the lignin breakdown products (LBPs) *p*-coumarate and coniferyl alcohol, and for the first time, bioplastics were produced from coniferyl alcohol. This study also reveals that *R. palustris* can create a copolymer called poly-3-hydroxybutyrate-co-hydroxyvalertae (PHBV) (Supplementary Fig. S1), which boosts the thermomechanical properties compared to PHB alone. A deep-dive analysis was conducted to gain fundamental understandings of the complex networks employed by *R. palustris* for PHB production from the LBPs compared to acetate and butyrate. Analyses included growth comparisons, optimal stress conditions for PHB/V production, PHB/V fractions produced over time, fluorometry analysis, transmission electron microscopy, and H_2 production. It was unclear as to why the LBPs produced significantly more PHB titer than acetate or butyrate despite providing the same carbon content on a carbon-to-carbon basis. Based on unique experimental findings from discrepancies in PHB/V titers, TEM, and H_2 production, we hypothesized that PHB production is highly dependent on the characteristics of the substrate utilized. Furthermore, Expression of genes in its PHB synthesis pathway has been observed to remain constant under different conditions[11,17], leading to the hypothesis that changes in PHB production are caused by metabolic differences between the conditions tested.

These unique experimental findings motivated the application of *iRpa940*[35], a recently developed GSMM of *R. palustris*, to identify the key metabolic factors controlling PHB production. *iRpa940* was chosen due to its ability to simulate growth under different conditions, including an array of organic acids (i.e., acetate, butyrate, fumarate, and succinate) and LBPs and very high correlation of model-predicted fluxes with experimental flux measurements. The model was also shown to capture the observed complex trade-offs between different metabolic modules required for *R. palustris* to maintain optimum redox balance. Hence, the GSMM was applied to uncover possible causes for these experimental findings and to offer engineering design strategies that optimize PHB production. Four major findings from the GSMM include (i) a very high AcCoA/CoA ratio is required to drive the thiolase reaction, (ii) substrates with high carbon uptake rates accumulate higher amounts of acyl-CoA, (iii) the rate through PhaB (reductase) is linearly dependent on the NADPH/NADP ratio, and (iv) PhaB will likely be rate-limiting even under optimal metabolic conditions due to the very low catalytic efficiency. These findings suggest novel engineering design strategies to optimize PHB production including choosing substrates that bypass the thiolase reaction (e.g. *p*-coumarate), utilizing high molecular weight substrates for high carbon uptake rates, and using highly reduced substrates. Furthermore, this study shows that renewable and abundant LBPs to be ideal candidates for PHB production. Ultimately, this study showcases how an integrated approach utilizing GSMMs can help identify key factors associated with a bioconversion that would have otherwise not been recognizable. The engineering design strategies derived from this integrated approach could be applied to other bacteria, advancing the replacement of petroleum-derived plastics with sustainable biopolymers.

Results and Discussion

Disparities in PHB/V titers from cells grown on various carbon sources

In our previous study, *R. palustris* was shown to grow on *p*-coumarate and produced PHB to a much higher titer than on acetate[1]. It was unclear as to why more PHB production was observed from the LBP *p*-coumarate compared to virtually no PHB production from acetate when providing the same carbon content for fermentation. To better understand how the choice of substrate impacts PHB production, we conducted growth and PHB production analyses on the LBP coniferyl alcohol (previously underreported) and compared performance from the LBPs to that of acetate and butyrate. Butyrate was compared to acetate on a carbon-to-carbon basis to test the impact on PHB titer from a more reduced substrate that bypasses the energy intensive keto-thiolase reaction. All substrates were supplemented with 10mM sodium bicarbonate unless specified otherwise, and this carbon content was factored into the analyses. *R. palustris* was indeed able to grow on the LBP coniferyl alcohol (Fig. 2A) and reached a significantly higher maximum optical density (OD) of 3.22 compared to *p*-coumarate (2.17), butyrate (0.41), and acetate (0.87). A higher maximum OD suggests more CO_2 is being utilized during the degradation of the LBPs compared to the other carbon sources[36,37]. Furthermore, the increased growth rates of the LBPs signify faster carbon uptake rates.

Before proceeding with PHB analysis between the carbon sources, a starvation analysis was conducted to decipher if nitrogen or phosphorous limitation yields more PHB since this has been shown previously to boost production[38]. Starvation analysis was conducted on *p*-coumarate and employed either nitrogen, phosphorus, or both nitrogen and phosphorous starvation conditions. Nitrogen starvation yielded a significantly higher PHB titer, and thus it was used to compare PHB production across the substrates (Fig. 2B).

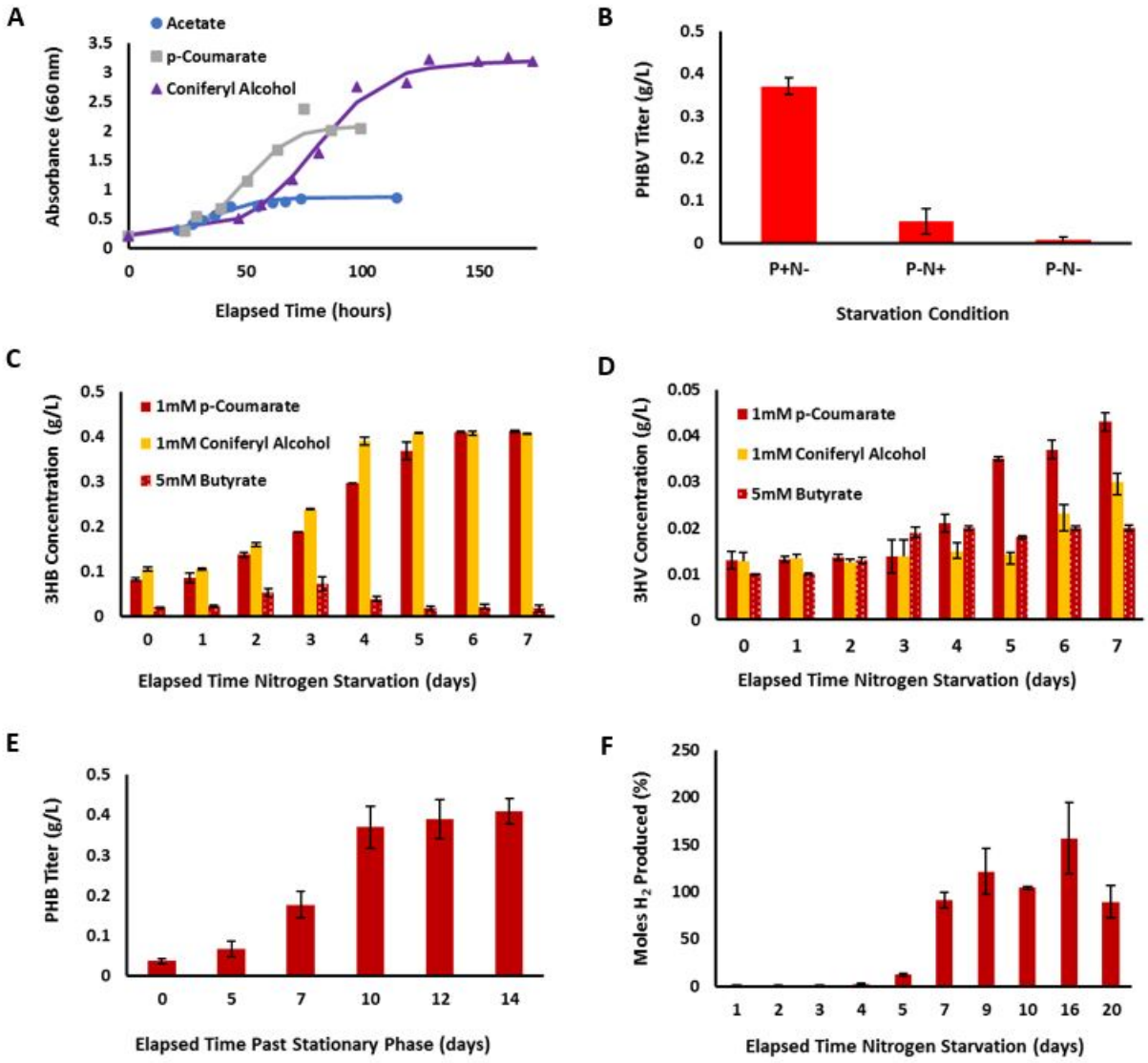

Fig. 2: Unique findings from experimental data that motivated application of the GSMM. (A) Anaerobic growth analyses. All substrates were supplemented with 10mM sodium bicarbonate. (B) Starvation condition analysis comparing nitrogen starvation, phosphorous starvation, and a combination of both nitrogen and phosphorus starvation. (C) Comparison of 3HB titers on LBPs vs. butyrate. (D) Comparison of 3HV titers on LBPs vs. butyrate. (E) PHB production from stationary phase (i.e. without resuspending in nitrogen-starved media). (F) Hydrogen production from 1mM *p*-coumarate after nitrogen starvation. All error bars represent the standard error for the population and are derived from the mean of biological triplicates for each data point.

Interestingly, the same maximum PHB titer (approximately 0.41 g/L) was observed for *p*-coumarate and coniferyl alcohol despite coniferyl alcohol having a higher carbon content (Fig. 2C). The carbon conversion efficiency for the maximum titer of 0.41 g/L (3.25 mM) PHB was calculated for 1 mM *p*-coumarate (Eq. 1) and 1 mM coniferyl alcohol (Eq. 2), yielding 68.4% and 65% respectively.

$$\frac{0.013\ moles\ carbon\ produced\ in\ PHB}{0.019\ moles\ carbon\ invested}\ x\ 100 = 68.4\%\ carbon\ conversion \quad (1)$$

$$\frac{0.013\ moles\ carbon\ produced\ in\ PHB}{0.02\ moles\ carbon\ invested}\ x\ 100 = 65\%\ carbon\ conversion \quad (2)$$

This study also shows for the first time that *R. palustris* produces PHBV, a copolymer of PHB that is less brittle. The LBPs and butyrate all fostered a 3-hydroxyvalerate (3HV) component that creates the copolymer PHBV (Fig 2D), with *p*-coumarate yielded the highest 3HV titer of approximately 0.04 g/L.

Transmission electron microscopy was conducted to image granules inside of the cells on the LBPs vs. acetate and revealed stark discrepancies between the LBPs and acetate as expected based on the measured titers. Virtually no granules were present inside cells grown on acetate, whereas there was an abundance of cells that contained a granule when grown on LBPs. Of note, one large granule is produced in the cells utilizing the LBPs, which indicates cytoplasmic space might be a major limiting factor for the maximum PHB titer as shown in *Halomonas bluephagenesis*[39]. A subsequent analysis was conducted to decipher PHB production on *p*-coumarate without nitrogen starving the cells (Fig. 2E). PHB production peaked at approximately 10 days past stationary phase with a similar maximum titer as that of the nitrogen-starved cells (0.41 g/L).

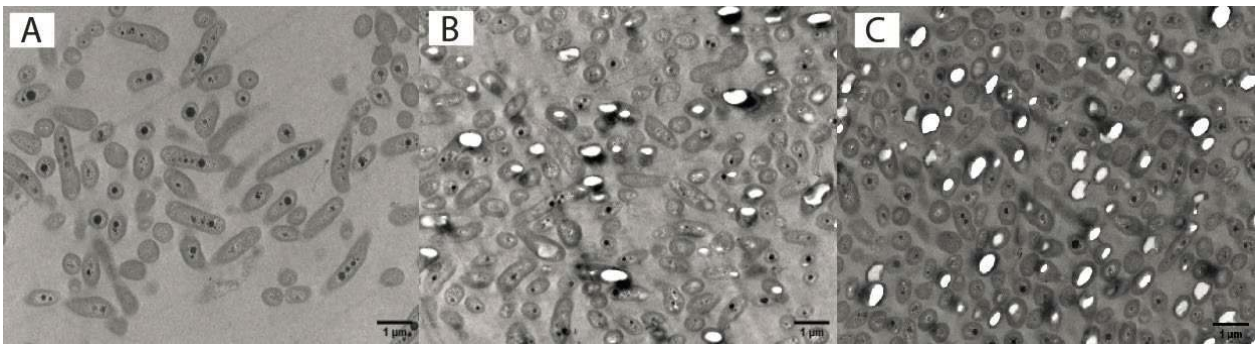

Fig. 3: Transmission Electron Microscopy (TEM). TEM images of *R. palustris* CGA009 cells grown anaerobically in photosynthetic media supplemented with (A) 10mM acetate and 10mM sodium bicarbonate, (B) 1mM *p*-coumarate and 10mM sodium bicarbonate, and (C) 1mM coniferyl alcohol and 10mM sodium bicarbonate. All samples were grown to mid-exponential phase, and subsequently nitrogen starved for five days. White inclusions inside the cytoplasm denote PHBV granules.

Tradeoffs between PHB and H_2 production

Hydrogen production was assessed on nitrogen-starved cells to compare the tradeoffs between PHB and H_2 production from 1 mM *p*-coumarate (Fig. 2F). Interestingly, the average moles of hydrogen produced began to significantly increase on day five of nitrogen starvation, which was when PHB production peaked. Since PHB production has been linked to reducing potential[17], we hypothesized that once the maximum PHB accumulated in the cells the reducing potential from the LBP is then funneled to hydrogen production. Thus, the reducing potential of the substrate is of note and needed to be investigated further with the application of the GSMM. Based on the unique experimental findings from the PHB titers, TEM, and H_2 production, we hypothesized that PHB production is highly dependent on the characteristics of the substrate utilized.

The GSMM was next employed to investigate the potential mechanisms behind these findings and identify specific design strategies that can be implemented to optimize PHB production. Due to the lack of kinetic parameters and concentration ranges for PHBV-producing reactions and their corresponding metabolites, the model was strictly used to investigate PHB production. However, since both monomer products (3-hydroxybutyrate and 3-hydroxyvalerate) are produced by the same enzymes, it is likely that the identified design strategies are applicable to both products.

Computational analysis of PHB production

Computational methods were employed to investigate the observed experimental findings. The main question that the GSMM intended to address was what underlying factors cause the observed disparity in PHB production between the tested carbon sources. More importantly, can a set of generalized design strategies for PHB overproduction be deduced by incorporating the observed experimental findings into a whole-cell metabolic modeling framework? To guide the analysis of the GSMM, a detailed thermo-kinetic study of the pathway was conducted to determine how the overall production rate of PHB is affected by the cell's metabolic state. The goal of this analysis was to identify the different metabolic factors (e.g., NADPH redox state) governing the activity of the PHB pathway. Growth simulations facilitated by the GSMM can then be used to determine how consumption of each substrate affects the identified factors and therefore the rate of PHB synthesis.

Thermo-kinetic analysis of the PHB pathway

The rate of an unregulated enzymatic reaction that follows Michaelis-Menten kinetics can be broken down into a product of three main constituents: (i) the enzyme's catalytic capacity (V^{max}), (ii) the reaction's thermodynamic driving force (γ), and (iii) enzyme substrate saturation (κ)[40].

This can be expressed mathematically as shown in Eq. 3:

$$v = V^{max} * \gamma * \kappa \quad (3)$$

where, the maximal rate of the reaction is determined by its catalytic efficiency and enzyme concentration ($V^{max} = [E]k_{cat}$). The thermodynamic driving force can take on values of 0 to 1 when the reaction is in the forward direction and -1 to 0 when the reaction is going in the reverse direction. Moreover, the enzyme saturation factor has a range of 0 to 1. Since the rate law, written in this form, is separable, the effect of each factor on the overall rate can be analyzed individually[40]. Starting with the first reaction in the pathway (PhaA), it was found that this reaction is significantly constrained thermodynamically (Fig. 4A). As described previously, the rate of the reaction was highly dependent on the acetyl-CoA/CoA ratio[13,14]. Surprisingly, the reaction was found to be infeasible under a ratio 12, which is relatively high compared to ratios observed in most bacteria (<5)[41–45]. This means that a significant accumulation of acetyl-CoA is required for thiolase to become thermodynamically viable and start forming acetoacetyl-CoA. This limitation is likely a major contributor to why no PHB was observed during growth on acetate, even after nitrogen starvation. On the other hand, the breakdown pathways of the other carbon substrates produced acetoacetyl-CoA as an intermediary metabolite (Fig. 5), therefore bypassing this thermodynamic obstacle. Moreover, changes to this ratio displayed a minimal effect on κ (Fig. 4A), meaning that during any given condition, the rate of the reaction, relative to Vmax, can be estimated solely based on γ (Fig. 4B). Due to the high thermodynamic burden of the PhaA reaction, substrates that breakdown into acetoacetyl-CoA as an intermediary metabolite could help maximize PHB production.

Interestingly, an opposite conclusion was reached during analysis of the reaction through acetoacetyl-CoA reductase (PhaB). Although both factors (γ and κ) contributed to the overall rate, substrate saturation was significantly more limiting (Fig. 4C). An increase in the NADPH/NADP ratio relieves the bottleneck through this reaction by increasing both the thermodynamic driving force and substrate saturation. Furthermore, the concentration of the main reaction product (3-hydroxybutyryl-CoA) has a pronounced effect on substrate saturation. The solid and dotted lines in Fig. 4C correspond to the minimum and maximum 3-hydroxybutyryl-CoA concentrations reported in literature[10,13]. The combined effect of both factors on the overall flux through the reaction is shown in Fig. 4D. Although the reaction is viable under different biologically relevant NADPH:NADP ratios, flux through PhaB is significantly hindered during high NADP(H) oxidation states (i.e., low NADPH:NADP ratios) due to the enzyme being sub-saturated (κ << 1). Finally, reports from previous kinetic studies had identified that PhaB's kinetic capacity (V^{max}) was notably lower than that of PhaA and PhaC[22,23], meaning that for steady-state PHB accumulation to occur, a relatively higher expression rate of this enzyme is required for the fluxes to be balanced. The implications of this difference in catalytic efficiency are discussed in the Supplementary Methods. Therefore, even under optimal metabolic conditions (high NADPH:NADP ratio), the catalytic inefficiency of the reductase enzyme may limit the overall rate of the PHB pathway.

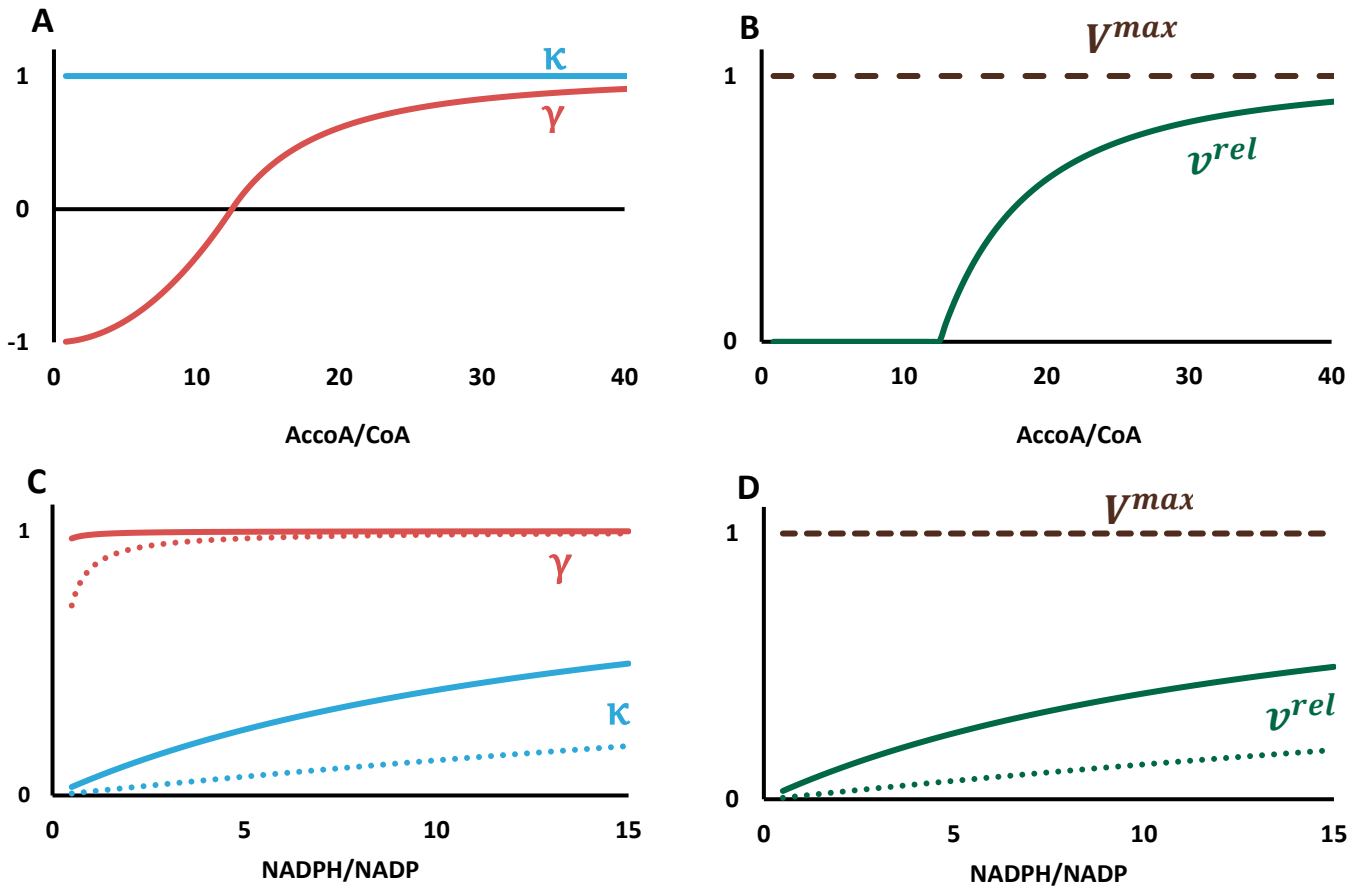

Fig. 4: Thermo-kinetic analysis of thiolase (PhaA) and reductase (PhaB) activity. Effect of the acetyl-CoA/CoA ratio on the reaction's (A) thermodynamic driving force (γ) and substrate saturation (κ) and (B) Overall rate relative to V^{max}. Effect of the NADPH/NADP ratio on the reaction's (C) thermodynamic driving force (γ) and substrate saturation (κ) and (D) Overall rate relative to V^{max}. Solid and dotted lines correspond to a 3-hydroxybutyryl-CoA concentration of 30 µM and 300 µM, respectively.

Genome- scale prediction of metabolic activity through fluorometry and iRpa940

To investigate the cause of the disparities between PHB production during growth on *p*-coumarate compared to that on butyrate, *iRpa940* model was employed to explore differences in the generation of both carbon and electron sources. It had been previously observed that the activity of *R. palustris'* metabolic network during anaerobic growth conditions can be predicted accurately if the rate of photosynthesis, or the electron transport rate (ETR), was known *a priori*[35]. When ^{13}C metabolic flux analysis (MFA) measurements are available, the ETR can be determined by fitting pFBA-generated flux predictions to those measured through MFA[35]. The ETR values during growth on acetate and butyrate were available *a priori*[35]. However, due to the absence of MFA measurements during growth on *p*-coumarate, pulse amplitude modulation (PAM) fluorometry was conducted to determine the relative ETR through cells growing on *p*-coumarate compared to those growing on acetate. First, ETR values predicted through MFA measurements[35] during growth on acetate and butyrate were validated. Based on the MFA measurements, the model had predicted that the ETR, and therefore the photosynthetic yield, was similar during growth on these two substrates[35]. Fluorometry measurements show that the photosynthetic yields are indeed similar (Fig. 6). These results gave confidence in the validity of subsequent model predictions. Next, PAM fluorometry was used to measure the photosynthetic yield during growth on *p*-coumarate. Interestingly, the ETR was found to be significantly higher during growth on *p*-coumarate compared to growth on acetate and butyrate (Fig. 6). These measurements provided the parameters required for the GSMM to simulate anaerobic growth on each of the carbon sources. Supplementary Figs. S2-4 shows the metabolic activity through the central metabolism during growth on the three substrates. Next, these predictions were used to compare how the generation rates of different metabolites participating in PHB synthesis varied between carbon sources.

A

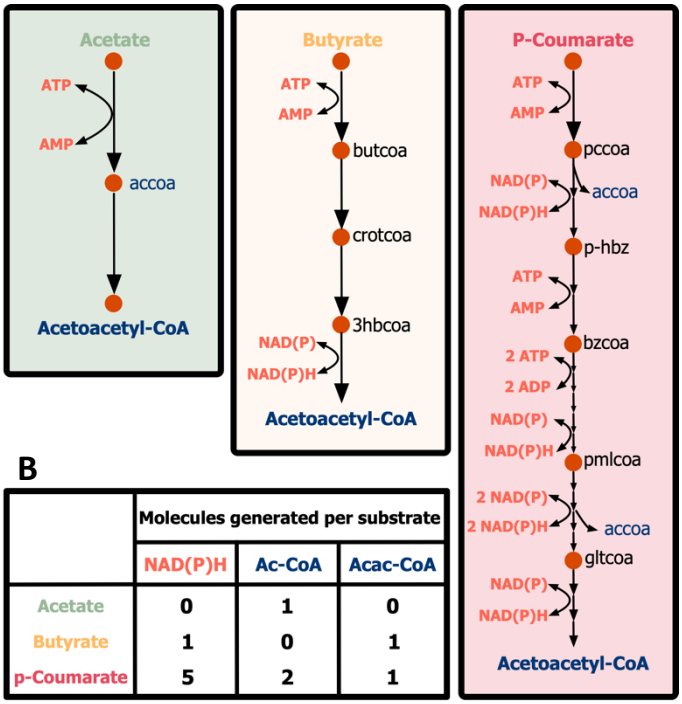

B

	Molecules generated per substrate		
	NAD(P)H	Ac-CoA	Acac-CoA
Acetate	0	1	0
Butyrate	1	0	1
p-Coumarate	5	2	1

Fig. 5: Substrate consumption of the three modeled carbon sources: acetate, butyrate, and *p*-coumarate depicting the (A) breakdown pathways and the (B) relevant cofactors and PHB precursors produced from each carbon source.

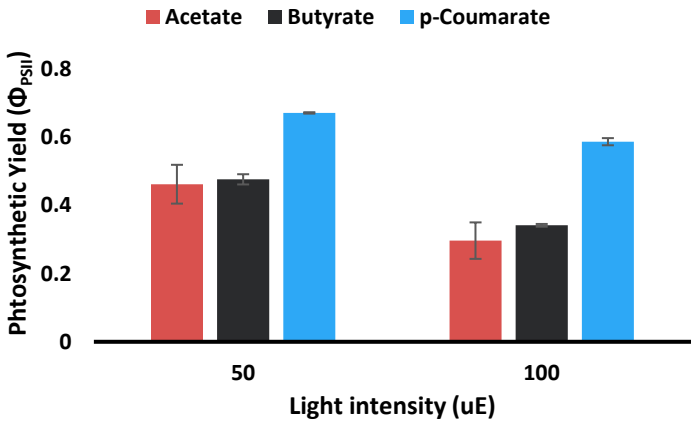

Fig. 6: Photosynthetic yields of *R. palustris* cells grown on different carbon sources as measured at 50 µE and 100 µE.

PHB synthesis within the context of metabolism

First, the overall generation rate of NAD(P)H was determined during growth on each carbon source based on the model-generated growth predictions (see Methods). The rationale behind this analysis was that a higher generation rate of reducing power results in a more reduced state and a higher driving force through the reductase (PhaB). It has also been reported that *R. palustris'* metabolism is constrained by its inability to oxidize cofactors through the electron transport chain due to the lack of a terminal electron acceptor[36,37], which forces it to utilize other routes such as carbon fixation, nitrogen fixation or PHB synthesis to accomplish this[37,46]. During steady-state growth, the rate at which cofactors are oxidized needs to be equivalent to the rate of reduction to avoid the accumulation of electrons. As can be seen from Fig. 7, growth on butyrate and *p*-coumarate generate approximately 40% and 95% more reducing equivalents compared to acetate, respectively. Since reduced cofactors (NAD(P)H) are generated during substrate breakdown, the differences in generation rates (Fig. 7) correspond to differences in substrate oxidation states, uptake rates, and breakdown pathways (Fig. 5). Furthermore, since both of these substrates (butyrate and *p*-coumarate), generate acetoacetyl-CoA during their breakdown, the redox state of their respective NADP(H) pool can be considered the rate-limiting factor for PHB production. It is noted that since biomass production is another major sink of electrons, this effect becomes more pronounced during nitrogen-starvation when biomass generation is halted. Results from this analysis indicate that the higher rate of NAD(P)H generation likely leads to a significantly more reduced intracellular state. In the closely related strain *R. palustris* TIE1, the measured NADPH:NADP ratio during anaerobic growth on butyrate was approximately 2[47]. Therefore, as indicated by the thermo-kinetic analysis, a higher ratio during growth on *p*-coumarate will lead to a higher rate through the reductase reaction in the PHB pathway.

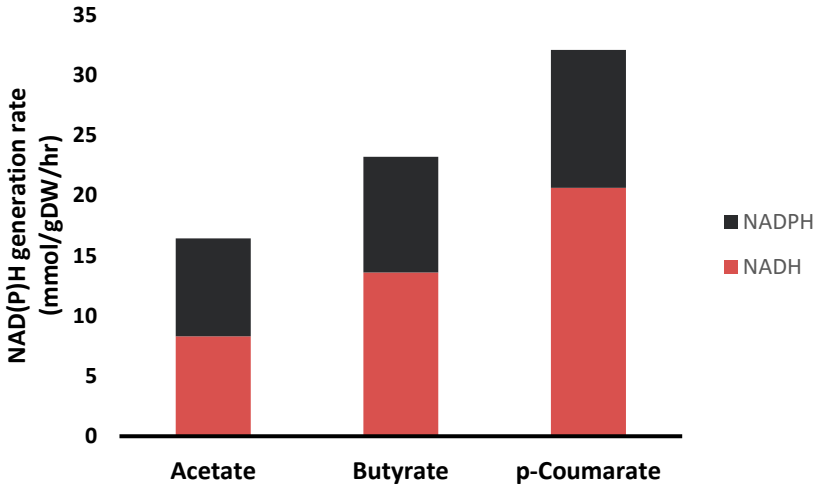

Fig. 7: Predicted reduction rates of the cofactors NAD and NADP during growth on acetate, butyrate, and *p*-coumarate.

During anaerobic growth conditions in which nitrogen fixation is not required, *R. palustris* utilizes CO_2 fixation through the Calvin Cycle as its primary electron sink[36,37]. Therefore, the rate of carbon fixation was expected to show a similar trend to that of NAD(P)H generation[36]. Indeed, as shown on Fig. 8, the relative rate of carbon fixation is proportional to the rate of reducing cofactors. Relative rates were calculated by normalizing the predicted CO_2 fixation rates by the rate predicted during growth on acetate. The predicted rates during growth on each carbon source are shown on the metabolic maps in Supplementary Figs. S2-4. Due to the high NAD(P)H generation rate during growth on *p*-coumarate, the model predicts a 3-fold increase in carbon fixation compared to growth on acetate (Fig. 8). However, due to known inefficiency of the carbon fixing enzyme Ribulose-1,5-bisphosphate carboxylase-oxygenase (RuBisCO)[48], it is plausible to postulate that kinetics of the RuBisCO enzyme do not permit such a high rate. Therefore, the cell would be required to store the remaining excess electrons in PHB, which is the only alternative electron sink under such conditions. It is also noted that model predictions indicate that both NAD(P)H generation and carbon fixation rates increase with increasing ETR during growth on any of the three substrates.

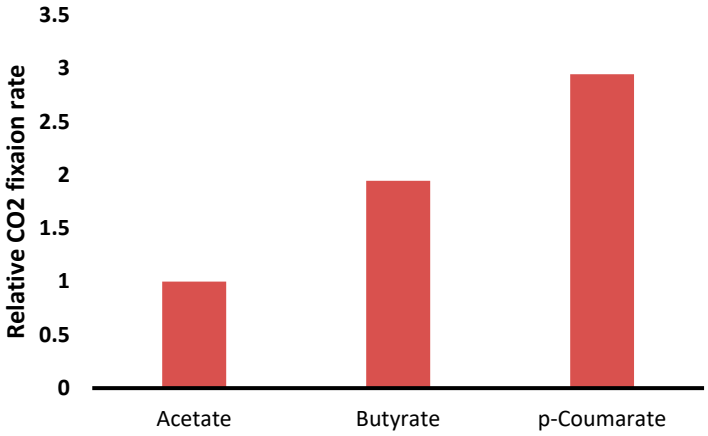

Fig. 8: Relative predicted rate of CO_2 fixation during growth on acetate, butyrate, and *p*-coumarate.

Finally, the model was used to investigate how utilization of each of the carbon substrates affected the rate of acetyl-CoA and acetoacetyl-CoA generation (Fig. 9). As previously described, although acetyl-CoA is considered to be the first metabolite in the PHB synthesis pathway, its conversion to acetoacetyl-CoA is thermodynamically very unfavorable. It was therefore hypothesized that exploring the rate of acetoacetyl-CoA generation may give a better indication of PHB production. Growth simulations on acetate showed that all of the consumed substrate was converted into acetyl-CoA before entering the central metabolic pathways through the TCA cycle. Since acetate assimilation into central metabolism does not produce acetoacetyl-CoA, model predictions indicate that only a small fraction of the starting carbon gets converted to this metabolite, while the majority is used to synthesize other biomass precursors and constituents. Conversely, consumption of butyrate mandates that all of the starting substrate goes through acetoacetyl-CoA before entering central metabolism. In fact, butyrate's breakdown pathway also goes through 3-hydroxybutyrate CoA (Fig. 5), which is the monomer form of PHB. Furthermore, due to the constitutive nature of the genes involved in PHB synthesis, generation of acetoacetyl-CoA during assimilation of the carbon source into central metabolism is expected to result in PHB production even under conditions when carbon or electron storage is not required. As shown in Fig. 2, PHB production is observed in cells growing even prior to nitrogen starvation. Finally, growth on *p*-coumarate results in relatively high generation rates of both acetyl- and acetoacetyl-CoA. Model analysis reveals that based on the measured growth rates, the rate of carbon uptake is 4.5-fold higher during growth on *p*-coumarate compared to acetate. Therefore, this analysis reveals that the basis behind the highly observed PHB production rate on *p*-coumarate is likely due to both an excess of carbon and electrons. It is likely that due to the large size of *p*-coumarate (and LBPs in general), the rate at which central metabolites are generated is too high to enter central metabolism, which is why PHB production can be observed even during exponential growth. Similar behavior has been observed in *E. coli* under high carbon uptake rates and has been referred to as Janusian growth[49].

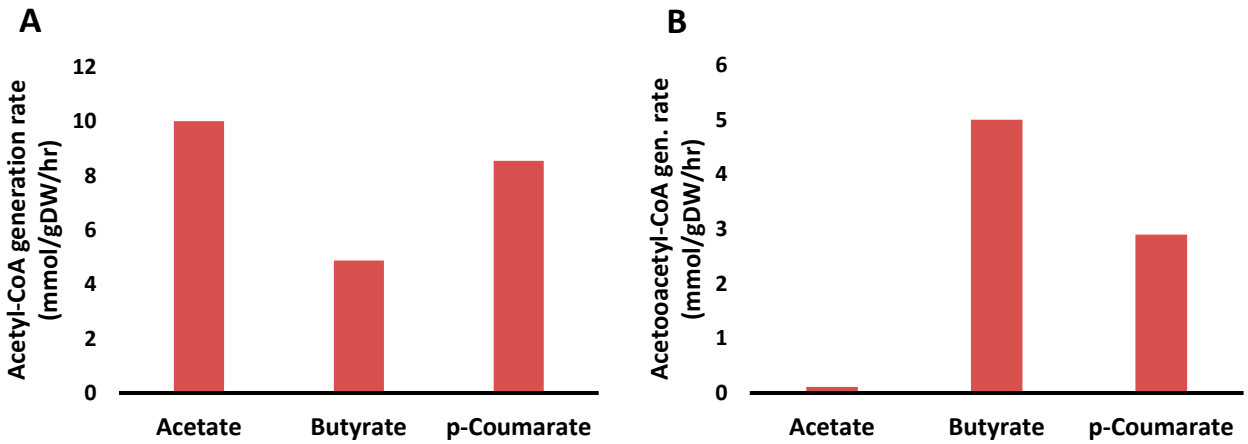

Fig. 9: Predicted generation rates of the first two substrates in the PHB pathway (acetyl-CoA (A) and acetoacetyl-CoA (B)) during growth on acetate, butyrate, and *p*-coumarate.

General design strategies for PHB production

These findings can be generalized into a set of design strategies for optimal PHB production. Due to the constitutive expression of the metabolic *pha* genes in *R. palustris*, changes in the intracellular metabolic state in the form of increased carbon and electron accumulation have a direct effect on the pathway's activity. Therefore, carbon sources used for PHB production should ideally have a high molecular weight and be more reduced than the organism's biomass. This will lead to the generation of an excess in both reducing agents (NAD(P)H) and carbon that can subsequently be shuttled towards PHB production. Moreover, the substrates should preferably produce acetoacetyl-CoA as part of their breakdown. This is necessary to bypass the extremely unfavorable first reaction of the PHB pathway. Based on these characteristics, LBPs such as *p*-coumarate and coniferyl alcohol appear to be ideal candidates for PHB production. Finally, under optimal metabolic conditions, it is expected that the catalytic efficiency of PhaB may play a limiting role in the overall rate (Supplementary Methods). Therefore, overexpression of *phaB* may be necessary to increase PHB production rates under such conditions. Most importantly, the generality of these design rules allows them to be applied to any PHB-producing microbe.

Conclusions

Novel design strategies for improved PHB production have been identified through an integrated experimental and computational approach. The unique findings from the metabolically versatile *R. palustris*, 1) significantly higher PHB production rates from LBPs, 2) PHB production without stress induction, 3) growth from coniferyl alcohol, 4) increased hydrogen production as PHB production peaks, 5) production of the copolymer PHBV, and 6) cytosolic space constricting continued PHB production, led to the hypothesis that PHB production was driven by the metabolic state of the cell. Utilizing *R. palustris'* ability to consume a wide array of substrates,

four carbon sources with different redox state (number of available electrons), size (number of carbons), and the consumption route taken to reach central metabolism were used to test this hypothesis. A metabolic modeling approach was then taken to gain a deeper understanding of the underlying factors causing the discrepancies in observed PHB production. Three main design strategies for optimizing PHB production regardless of the producing host emerged.

First, PHB production efforts should utilize carbon sources that can bypass the thiolase reaction. Modeling results indicated that under normal Acetyl-CoA:CoA ratios, the first reaction in the PHB synthesis pathway was infeasible. This result explains, at least partly, why no PHB production was observed during growth on acetate. On the other hand, growth on butyrate and *p*-coumarate does not require this reaction for PHB production, as both substrates produce acetoacetyl-CoA as part of their consumption pathway. Although the assimilation route of coniferyl alcohol is not known, it is likely that, breakdown of this substrate produces acetoacetyl-CoA as part of its consumption pathway, similar to *p*-coumarate. Second, carbon substrates used for PHB production should be more reduced than the cell's biomass. Model analysis indicates that activity of the acetoacetyl-CoA reductase is highly dependent on the redox state of NADPH, especially under physiologically relevant NADPH:NADP ratios. The importance of this result is magnified due to the inherently low catalytic efficiency of this enzyme. Therefore, use of a highly reduced substrate is predicted to lead to a higher NADPH:NADP ratio and therefore enhance the rate through this reaction. Third, the utilized substrates should have high molecular weights, or a relatively large number of carbons. Growth measurements and model predictions indicate that the relatively large size of *p*-coumarate and coniferyl alcohol leads to a higher carbon uptake rate. At the observed uptake rates, catalytically inefficient enzymes within central metabolism such as RuBisCO are likely to operate close to their maximum capacity, leading to an increased production of storage metabolites such as PHB. The increased uptake rate is also what leads to the predicted generation rates of NAD(P)H and acyl-CoAs being significantly higher during growth on *p*-coumarate. As evident from the characteristics of *p*-coumarate and coniferyl alcohol, and from the measured PHB profiles associated with them, it appears that LBPs are ideal substrates for PHB production and can lead to an economically viable process for PHB production. Overall, this study showcases how an integrated experimental-modeling approach can identify a set of novel engineering design strategies associated with sustainable biopolymer production, thus advancing the replacement of petroleum-derived plastics.

Methods

Growth curves and PHB/V production

R. palustris seed culture preparation, growth curves, and PHB production were performed as described[9]. Briefly, seed cultures were diluted to an optical density (660 nm) of 0.2 and grown anaerobically at 30°C with 100 µE white light in the same media as the seed cultures but with different carbon sources. Instead of the 20mM sodium acetate used for seed cultures, either

10mM sodium acetate, 5mM sodium butyrate, 1mM *p*-coumarate, or 1mM coniferyl alcohol were supplied. Growth data were fitted to a modified logarithmic growth model as described previously[9,34].

Once growth parameters were determined from the growth models (Fig. 2), cultures were grown to mid-exponential in the respective conditions (except when specified otherwise) and subsequently nitrogen starved as described previously[9]. Briefly, for nitrogen starvation the anaerobic vials were centrifuged to generate a pellet, the supernatant was discarded, and the pellet was resuspended in media with the desired carbon sources without ammonium sulfate as a nitrogen source.

PHB/V quantification via gas-chromatography mass spectrometry (GC-MS)

PHB/V extraction and quantification was conducted as described previously[1]. A triplicate of anaerobic culture vials was harvested from each condition for analysis at the desired growth phase (i.e., mid-exponential or stationary phase) and after each day of nitrogen starvation. Each vial was subjected to acidic methanolysis, and PHB/V was quantified with conventional GC-MS as described[1]. External standards were created from serial dilutions of sodium 3-hydroxybutyrate or (−)-Methyl (R)-3-hydroxyvalerate (Sigma-Aldrich™).

Hydrogen quantification via gas chromatography-thermal conductivity detector (GC-TCD)

Samples were nitrogen-starved as described above. Precisely 3 mL of the nitrogen-starved culture was placed into a 10 mL air-tight glass vial with 18 mm headspace (Thermo Scientific®). The glass vials were immediately closed with air-tight magnetic screw caps that contained self-sealing septums (Thermo Scientific®). The vials were flushed with argon for 30 mins by piercing the septums with a needle attached to the argon tank and another needle for outlet gas. Once the samples were purged with argon, they were placed into the lighted growth chamber until testing, using the same light intensity, temperature, and shaking as described above. Hydrogen quantification was conducted by drawing 500 µL of gas from the headspace into an airtight, fixed needle syringe (Thermo Scientific®) and manually injected into the thermal conductivity detector (TCD) (Thermo Scientific Trace 1300) of the gas chromatograph. The characterization methods were the same as described in Tiryaki and Irmak, 2020, including the carrier gas, column, and GC parameters[50]. A gas mixture of known composition was used as a standard, and had the same composition as described[50].

Transmission Electron Microscopy (TEM)

To visualize the PHB/V granule(s) inside the cell, samples from 10mM acetate, 1mM *p*-coumarate, and 1mM coniferyl alcohol after five days of nitrogen starvation were subjected to TEM. The bacteria were fixed in 2% glutaraldehyde and 1.5% paraformaldehyde in 100mM sodium cacodylate buffer for > 1 hour at room temperature and then 4°C overnight. The samples were washed in sodium cacodylate buffer three times (10 min each) and post-fixed in 1% osmium tetroxide in deionized water at room temperature for one hour. After washing in water twice,

the samples were dehydrated through an ethanol series and embedded in Spurr medium using a conventional TEM processing protocol. Ultrathin sections were cut using a Leica UC7 ultramicrotome and stained with 1% uranyl acid and 1% lead citrate. Images were collected using a Hitachi H7500 TEM at the Microscopy Core Research Facility of the Center for Biotechnology, University of Nebraska-Lincoln.

Pulse Amplitude Modulation (PAM) Fluorometry

PAM fluorometry was conducted using the LI-6800 Portable Photosynthesis System, Software Version 1.4. LI-COR, Inc. to determine the photosynthetic yield (Φ_{PSII}) following the procedure developed by Ritchie et al.[51–55]. Briefly, anaerobically growing cells were centrifuged during the mid-exponential phase and re-suspended in 400 µL of PM media[56]. Precisely 250 µL of cell suspension was then uniformly pipetted onto a Whatman® glass fiber disk and air-dried for 20 minutes at room temperature. Next, the fiber disks were dark-adapted in an opaque container for 10-30 minutes and subsequently placed in the chamber of the LI-6800's multiphase flash fluorometer. Both the measuring and actinic light sources were set to ~465 nm (blue light)[52]. After setting the irradiance, the cells require approximately 15 minutes to reach a new steady-state (characterized by constant fluorescence), at which time a saturating light pulse is introduced to measure Φ_{PSII}[57]. Since the electron transport rate (ETR) is proportional to Φ_{PSII}[51,57] the relative photosynthetic rates during growth on any two conditions can be inferred from the relative photosynthetic yields (see eqn. 11).

Thermo-kinetic analysis

The rate law of a bi-molecular reaction can be re-written into the separable form below, as derived[40]:

$$v = Ek_{cat}^{+}\left(\frac{s/K_s}{1 + s/K_s + p/K_p}\right)\left(1 - e^{\Delta_r G\,'/RT}\right) \quad (4)$$

Where the first factor refers to the enzyme's catalytic capacity (V^{max}):

$$V^{max} = Ek_{cat}^{+} \quad (5)$$

The second term refers to the fractional substrate saturation (κ):

$$\kappa = \frac{s/K_s}{1 + s/K_s + p/K_p} \quad (6)$$

The third factor denotes the thermodynamic driving force (γ):

$$\gamma = 1 - e^{\Delta_r G'/RT} \quad (7)$$

The Gibbs free energy of a reaction ($\Delta_r G'$) can be calculated from the standard Gibbs free energy ($\Delta_r G'^{o}$) and the metabolite concentrations (or product to substrate ratios) [40]:

$$\Delta_r G' = \Delta_r G'^o + RTln\left(\frac{P}{S}\right) \quad (8)$$

The $\Delta_r G'^o$ values of the thiolase (PhaA) and reductase (PhaB) reactions were calculated using the component contribution method[58]. For thiolase, the acetoacetyl-concentration was set to the minimum physiological concentration of 1 µM[58] and the acetyl-CoA:CoA ratio was sampled to determine its effect on γ. For reductase, simulations were conducted using 3-hydroxybutyryl-CoA concentrations of 30 µM and 300 µM to capture the range of reported concentrations[10]. The NADPH:NADP ratio was sampled to determine its effect on γ.

Michaelis constants (K_s and K_p) used during simulation were reported for the soil bacterium *Cupriavidus necator*[10] as no values have been reported for *R. palustris*. Due to the high homology of both PhaA and PhaB (E value < 10^{-80}) between the two organisms, the substrate saturation effects were assumed to be similar. Supplementary Tables S1-S2 contain the parameters used in this analysis and the references they were obtained from.

GSMM simulations

Parsimonious Flux Balance Analysis (pFBA)[59] was used to simulate growth under different environmental conditions. pFBA is analogous to FBA but adds a second objective that minimizes the sum of all reaction fluxes. The two objectives were reformulated into one function through objective tilting[60] as displayed below.

$$Maximize\ v_{biomass} - 0.0001 \sum_{j \in J - v_{biomass}} v_j$$

$$subject\ to$$

$$\sum_{j \in J} S_{ij}.v_j = 0 \ \forall\, i \in I \quad (9)$$

$$LB_j \leq v_j \leq UB_j \ \forall\, j \in J \quad (10)$$

Where *I* and *J* are the sets of metabolites and reactions in the model, respectively. S_{ij} is the stoichiometric coefficient of metabolite *i* in reaction *j* and v_j is the flux value of reaction *j*. Parameters LB_j and UB_j denote the minimum and maximum allowable fluxes for reaction *j*, respectively. $v_{biomass}$ is the flux of the biomass reaction which mimics the cellular growth rate.

The rate through the photosynthetic electron transport reaction PSII (light-induced reduction of quinol) was fixed based on previous analysis for growth on acetate and butyrate[35]. The rate of this reaction during growth simulations on *p*-coumarate was calculated based on the relative photosynthetic yield (Φ_{PSII}) between *p*-coumarate and acetate:

$$v_{PSII}^{pC} = v_{PSII}^{ace} \frac{\Phi_{PSII}^{\mathrm{pC}}}{\Phi_{PSII}^{\mathrm{ace}}} \quad (11)$$

Where "pC" and "ace" refer to *p*-coumarate and acetate, respectively.

Finally, the generation rate of a metabolite *k* (e.g., acetyl-CoA) was calculated using Eq. 12 below:

$$genRate_k = \sum_{j \in J} v_j \;\; \forall\, j \in J \quad s.t.\; S_{kj} > 0 \quad (12)$$

Statistical Methods

Independent, two-tailed *t* tests were conducted to decipher statistically significant differences in maximum optical densities between acetate vs. *p*-coumarate, acetate vs. coniferyl alcohol, and *p*-coumarate vs. coniferyl alcohol. Similarly, *t* tests were conducted to compare maximum PHB titers between *p*-coumarate and coniferyl alcohol at 5 days of nitrogen starvation. Paired, one-tailed t-tests were conducted to decipher the time of maximum PHB production from *p*-coumarate and coniferyl alcohol. For example, a paired *t* test was conducted between Days 5 and 6 nitrogen starvation on *p*-coumarate to decipher the time of maximum PHB production. All *t* tests were conducted with a 95% confidence level ($\alpha = 0.05$).

Acknowledgments

We gratefully acknowledge funding support from National Science Foundation (NSF) CAREER grant (25-1106-0039-001), Nebraska Center for Energy Science and Research grants (26-1217-0020-403 and 26-1217-0020-413), National Science Foundation (NSF) EPSCoR Center for Root and Rhizobiome Innovation grant (25-1215-0139-025), NSF MCB grant (25-1215-0175-001), and U.S. Department of Agriculture National Institute of Food and Agriculture (USDA-NIFA) Postdoctoral Fellowship (2019-67012-29632). We extend special thanks to Dianna Long and Mark Kathol for sample collection at difficult times, and to Ehsan Zamani for ultrasonication. Additionally, we extend thanks to Dr. You Zhou at the University of Nebraska-Lincoln Microscopy Core Facility and Mr. Dirk Anderson at the University of Nebraska-Lincoln Flow Cytometry Core Facility for providing guidance for running the experiments. We are also thankful to Anjeza Erickson and Dr. Sibel Irmak at the Industrial Agricultural Products Center for providing support with GC-MS and hydrogen analysis. Finally, we would like to thank Jeremy Hiller at the Institute of Agriculture and Natural Resources and Dr. Taity Changa for providing and assisting with the photosynthesis fluorometry system.

Author Statement

Adil Alsiyabi: Conceptualization, Methodology, Software, Formal Analysis, Investigation, Writing - Original Draft, Resources, Data Curation, Visualization. **Brandi Brown:** Conceptualization, Methodology, Software, Formal Analysis, Investigation, Writing - Original Draft, Resources, Data

Curation, Visualization. **Cheryl Immethun:** Resources, Supervision, Writing - Review & Editing. **Mark Wilkins:** Resources, Funding acquisition, Supervision, Writing - Review & Editing. **Rajib Saha:** Resources, Funding acquisition, Supervision, Writing - Review & Editing.

Data Availability

All data in this study are available from the corresponding authors upon request. The code to recreate iRpa940 simulation results and the thermo-kinetic analysis are available at https://github.com/ssbio/Alsiyabi&Brown_et_al.git

References

1. Brown, B., Immethun, C., Wilkins, M. & Saha, R. Rhodopseudomonas palustris CGA009 polyhydroxybutyrate production from a lignin aromatic and quantification via flow cytometry. *Bioresour. Technol. Reports* (2020) doi:10.1016/j.biteb.2020.100474.
2. Medeiros Garcia Alcântara, J. *et al.* Current trends in the production of biodegradable bioplastics: The case of polyhydroxyalkanoates. *Biotechnology Advances* (2020) doi:10.1016/j.biotechadv.2020.107582.
3. Kleiner, M. *et al.* Metaproteomics of a gutless marine worm and its symbiotic microbial community reveal unusual pathways for carbon and energy use. *Proc. Natl. Acad. Sci. U. S. A.* (2012) doi:10.1073/pnas.1121198109.
4. Li, Z., Yang, J. & Loh, X. J. Polyhydroxyalkanoates: Opening doors for a sustainable future. *NPG Asia Materials* (2016) doi:10.1038/am.2016.48.
5. Chen, G. Q. A microbial polyhydroxyalkanoates (PHA) based bio- and materials industry. *Chem. Soc. Rev.* (2009) doi:10.1039/b812677c.
6. Chen, G. Q. & Zhang, J. Microbial polyhydroxyalkanoates as medical implant biomaterials. *Artif. Cells, Nanomedicine Biotechnol.* (2018) doi:10.1080/21691401.2017.1371185.
7. Chen, G.-Q., Chen, X.-Y., Wu, F.-Q. & Chen, J.-C. Polyhydroxyalkanoates (PHA) toward cost competitiveness and functionality. *Adv. Ind. Eng. Polym. Res.* (2020) doi:10.1016/j.aiepr.2019.11.001.
8. Lopar, M. *et al.* Five-step continuous production of PHB analyzed by elementary flux, modes, yield space analysis and high structured metabolic model. *Biochem. Eng. J.* (2013) doi:10.1016/j.bej.2013.07.003.
9. Chen, G.-Q. & Jiang, X.-R. Engineering bacteria for enhanced polyhydroxyalkanoates (PHA) biosynthesis. *Synth. Syst. Biotechnol.* **2**, 192–197 (2017).
10. Leaf, T. A. & Srienc, F. Metabolic modeling of polyhydroxybutyrate biosynthesis. *Biotechnol. Bioeng.* **57**, 557–570 (1998).

11. Ranaivoarisoa, T. O., Singh, R., Rengasamy, K., Guzman, M. S. & Bose, A. Towards sustainable bioplastic production using the photoautotrophic bacterium Rhodopseudomonas palustris TIE-1. *J. Ind. Microbiol. Biotechnol.* **46**, 1401–1417 (2019).

12. Tyo, K. E. J., Fischer, C. R., Simeon, F. & Stephanopoulos, G. Analysis of polyhydroxybutyrate flux limitations by systematic genetic and metabolic perturbations. *Metab. Eng.* **12**, 187–195 (2010).

13. van Wegen, R. J., Lee, S.-Y. & Middelberg, A. P. J. Metabolic and kinetic analysis of poly(3-hydroxybutyrate) production by recombinant Escherichia coli. *Biotechnol. Bioeng.* **74**, 70–81 (2001).

14. Kocharin, K., Chen, Y., Siewers, V. & Nielsen, J. Engineering of acetyl-CoA metabolism for the improved production of polyhydroxybutyrate in Saccharomyces cerevisiae. *AMB Express* **2**, 52 (2012).

15. Sekar, K. & Tyo, K. E. J. Regulatory effects on central carbon metabolism from poly-3-hydroxybutryate synthesis. *Metab. Eng.* **28**, 180–189 (2015).

16. Uchino, K., Saito, T., Gebauer, B. & Jendrossek, D. Isolated Poly(3-Hydroxybutyrate) (PHB) Granules Are Complex Bacterial Organelles Catalyzing Formation of PHB from Acetyl Coenzyme A (CoA) and Degradation of PHB to Acetyl-CoA. *J. Bacteriol.* **189**, 8250 LP – 8256 (2007).

17. McKinlay, J. B. *et al.* Non-growing Rhodopseudomonas palustris Increases the Hydrogen Gas Yield from Acetate by Shifting from the Glyoxylate Shunt to the Tricarboxylic Acid Cycle* *Experimental aspects of this research were supported equally by the Division of Chemical Sciences,. *J. Biol. Chem.* **289**, 1960–1970 (2014).

18. Centeno-Leija, S. *et al.* Improving poly-3-hydroxybutyrate production in Escherichia coli by combining the increase in the NADPH pool and acetyl-CoA availability. *Antonie Van Leeuwenhoek* **105**, 687–696 (2014).

19. Sacomboio, E. N. M. *et al.* The transcriptional regulator NtrC controls glucose-6-phosphate dehydrogenase expression and polyhydroxybutyrate synthesis through NADPH availability in Herbaspirillum seropedicae. *Sci. Rep.* **7**, 13546 (2017).

20. Chohan, S. N. & Copeland, L. Acetoacetyl Coenzyme A Reductase and Polyhydroxybutyrate Synthesis in Rhizobium(Cicer) sp. Strain CC 1192. *Appl. Environ. Microbiol.* **64**, 2859 LP – 2863 (1998).

21. Lee, I. Y., Kim, M. K., Park, Y. H. & Lee, S. Y. Regulatory effects of cellular nicotinamide nucleotides and enzyme activities on poly(3-hydroxybutyrate) synthesis in recombinant Escherichia coli. *Biotechnol. Bioeng.* **52**, 707–712 (1996).

22. Wang, F. & Lee, S. Y. Production of poly(3-hydroxybutyrate) by fed-batch culture of filamentation-suppressed recombinant Escherichia coli. *Appl. Environ. Microbiol.* **63**, 4765–4769 (1997).

23. Sim, S. J. *et al.* PHA synthase activity controls the molecular weight and polydispersity of polyhydroxybutyrate in vivo. *Nat. Biotechnol.* **15**, 63–67 (1997).

24. Islam, M. M. & Saha, R. Computational Approaches on Stoichiometric and Kinetic Modeling for Efficient Strain Design BT - Synthetic Metabolic Pathways: Methods and Protocols. in (eds. Jensen, M. K. & Keasling, J. D.) 63–82 (Springer New York, 2018). doi:10.1007/978-1-4939-7295-1_5.

25. Fondi, M. & Liò, P. Genome-Scale Metabolic Network Reconstruction BT - Bacterial Pangenomics: Methods and Protocols. in (eds. Mengoni, A., Galardini, M. & Fondi, M.) 233–256 (Springer New York, 2015). doi:10.1007/978-1-4939-1720-4_15.

26. Saha, R., Chowdhury, A. & Maranas, C. D. Recent advances in the reconstruction of metabolic models and integration of omics data. *Curr. Opin. Biotechnol.* **29**, 39–45 (2014).

27. Orth, J. D., Thiele, I. & Palsson, B. Ø. What is flux balance analysis? *Nat. Biotechnol.* **28**, 245–248 (2010).

28. Park, J. M., Kim, T. Y. & Lee, S. Y. Genome-scale reconstruction and in silico analysis of the Ralstonia eutropha H16 for polyhydroxyalkanoate synthesis, lithoautotrophic growth, and 2-methyl citric acid production. *BMC Syst. Biol.* **5**, 101 (2011).

29. Bordel, S., Rojas, A. & Muñoz, R. Reconstruction of a Genome Scale Metabolic Model of the polyhydroxybutyrate producing methanotroph Methylocystis parvus OBBP. *Microb. Cell Fact.* **18**, 104 (2019).

30. Bordel, S. *et al.* Genome scale metabolic modeling reveals the metabolic potential of three Type II methanotrophs of the genus Methylocystis. *Metab. Eng.* **54**, 191–199 (2019).

31. Tajparast, M. & Frigon, D. Predicting the accumulation of storage compounds by Rhodococcus jostii RHA1 in the feast-famine growth cycles using genome-scale flux balance analysis. *PLoS One* **13**, e0191835–e0191835 (2018).

32. Austin, S. *et al.* Metabolism of Multiple Aromatic Compounds in Corn Stover Hydrolysate by Rhodopseudomonas palustris. *Environ. Sci. Technol.* (2015) doi:10.1021/acs.est.5b02062.

33. Harwood, C. S. & Gibson, J. Anaerobic and aerobic metabolism of diverse aromatic compounds by the photosynthetic bacterium Rhodopseudomonas palustris. *Appl. Environ. Microbiol.* (1988) doi:10.1128/aem.54.3.712-717.1988.

34. Larimer, F. W. *et al.* Complete genome sequence of the metabolically versatile photosynthetic bacterium Rhodopseudomonas palustris. *Nat. Biotechnol.* **22**, 55–61 (2004).

35. Alsiyabi, A., Immethun, C. M. & Saha, R. Modeling the Interplay between Photosynthesis, CO2 Fixation, and the Quinone Pool in a Purple Non-Sulfur Bacterium. *Sci. Rep.* **9**, 12638

(2019).

36. McKinlay, J. B. & Harwood, C. S. Carbon dioxide fixation as a central redox cofactor recycling mechanism in bacteria. *Proc. Natl. Acad. Sci.* **107**, 11669 LP – 11675 (2010).

37. McKinlay, J. B. & Harwood, C. S. Calvin cycle flux, pathway constraints, and substrate oxidation state together determine the H2 biofuel yield in photoheterotrophic bacteria. *MBio* **2**, e00323-10 (2011).

38. Wen, Q., Chen, Z., Tian, T. & Chen, W. Effects of phosphorus and nitrogen limitation on PHA production in activated sludge. *J. Environ. Sci.* (2010) doi:10.1016/S1001-0742(09)60295-3.

39. Shen, R., Ning, Z. Y., Lan, Y. X., Chen, J. C. & Chen, G. Q. Manipulation of polyhydroxyalkanoate granular sizes in Halomonas bluephagenesis. *Metab. Eng.* (2019) doi:10.1016/j.ymben.2019.03.011.

40. Noor, E., Flamholz, A., Liebermeister, W., Bar-Even, A. & Milo, R. A note on the kinetics of enzyme action: A decomposition that highlights thermodynamic effects. *FEBS Lett.* **587**, 2772–2777 (2013).

41. Gameiro, D. *et al.* Computational resources and strategies to construct single-molecule metabolic models of microbial cells. *Brief. Bioinform.* **17**, 863–876 (2016).

42. Park, J. O. *et al.* Metabolite concentrations, fluxes and free energies imply efficient enzyme usage. *Nat. Chem. Biol.* **12**, 482–489 (2016).

43. Bennett, B. D. *et al.* Absolute metabolite concentrations and implied enzyme active site occupancy in Escherichia coli. *Nat. Chem. Biol.* **5**, 593–599 (2009).

44. Thauer, R. K., Jungermann, K. & Decker, K. Energy conservation in chemotrophic anaerobic bacteria. *Bacteriol. Rev.* **41**, 100–180 (1977).

45. CHOHNAN, S., IZAWA, H., NISHIHARA, H. & TAKAMURA, Y. Changes in Size of Intracellular Pools of Coenzyme A and Its Thioesters in Escherichia coli K-12 Cells to Various Carbon Sources and Stresses. *Biosci. Biotechnol. Biochem.* **62**, 1122–1128 (1998).

46. McKinlay, J. B. Systems Biology of Photobiological Hydrogen Production by Purple Non-sulfur Bacteria BT - Microbial BioEnergy: Hydrogen Production. in (eds. Zannoni, D. & De Philippis, R.) 155–176 (Springer Netherlands, 2014). doi:10.1007/978-94-017-8554-9_7.

47. Guzman, M. S. *et al.* Phototrophic extracellular electron uptake is linked to carbon dioxide fixation in the bacterium Rhodopseudomonas palustris. *Nat. Commun.* **10**, 1355 (2019).

48. Cummins, P. L., Kannappan, B. & Gready, J. E. Directions for Optimization of Photosynthetic Carbon Fixation: RuBisCO's Efficiency May Not Be So Constrained After All . *Frontiers in Plant Science* vol. 9 183 (2018).

49. O'Brien, E. J., Lerman, J. A., Chang, R. L., Hyduke, D. R. & Palsson, B. Ø. Genome-scale

models of metabolism and gene expression extend and refine growth phenotype prediction. *Mol. Syst. Biol.* **9**, 693 (2013).

50. Tiryaki, O. N. & Irmak, S. Evaluation of various corn variety kernels for hydrogen gas production by APR. *Biomass and Bioenergy* (2020) doi:10.1016/j.biombioe.2020.105480.

51. Phongjarus, N., Suvaphat, C., Srichai, N. & Ritchie, R. J. Photoheterotrophy of photosynthetic bacteria (Rhodopseudomonas palustris) growing on oil palm and soybean cooking oils. *Environ. Technol. Innov.* **10**, 290–304 (2018).

52. Ritchie, R. J. The Use of Solar Radiation by the Photosynthetic Bacterium, Rhodopseudomonas palustris: Model Simulation of Conditions Found in a Shallow Pond or a Flatbed Reactor. *Photochem. Photobiol.* **89**, 1143–1162 (2013).

53. Ritchie, R. J. & Mekjinda, N. Measurement of photosynthesis using PAM technology in a purple sulfur bacterium Thermochromatium tepidum (Chromatiaceae). *Photochem. Photobiol.* **91**, 350–358 (2015).

54. Ritchie, R. J. Fitting light saturation curves measured using modulated fluorometry. *Photosynth. Res.* **96**, 201–215 (2008).

55. Ritchie, R. J. & Larkum, A. W. D. Modelling photosynthesis in shallow algal production ponds. *Photosynthetica* **50**, 481–500 (2012).

56. Kim, M.-K. & Harwood, C. S. Regulation of benzoate-CoA ligase in Rhodopseudomonas palustris. *FEMS Microbiol. Lett.* **83**, 199–203 (1991).

57. Maxwell, K. & Johnson, G. N. Chlorophyll fluorescence—a practical guide. *J. Exp. Bot.* **51**, 659–668 (2000).

58. Noor, E., Haraldsdóttir, H. S., Milo, R. & Fleming, R. M. T. Consistent estimation of Gibbs energy using component contributions. *PLoS Comput. Biol.* **9**, e1003098–e1003098 (2013).

59. Lewis, N. E. *et al.* Omic data from evolved E. coli are consistent with computed optimal growth from genome-scale models. *Mol. Syst. Biol.* **6**, 390 (2010).

60. Feist, A. M. *et al.* Model-driven evaluation of the production potential for growth-coupled products of Escherichia coli. *Metab. Eng.* **12**, 173–186 (2010).

Figures

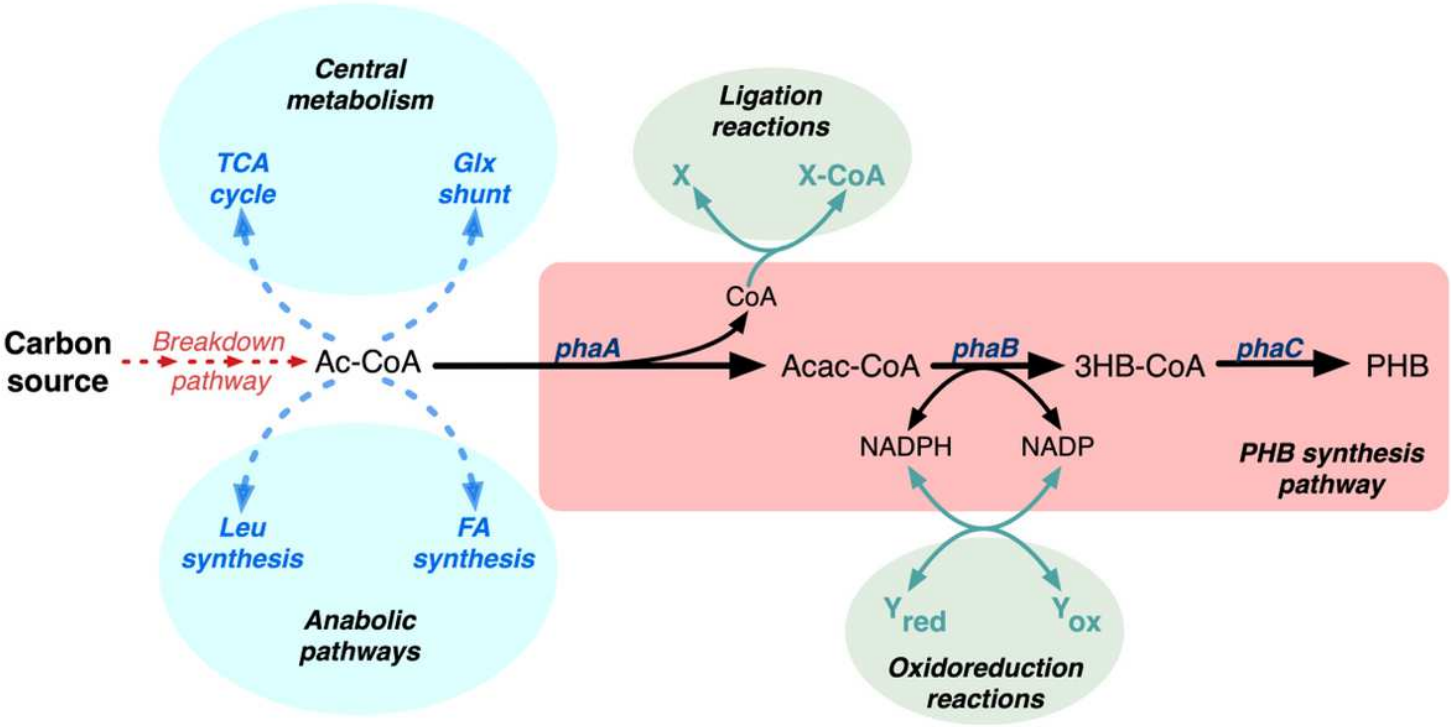

Figure 1

PHB synthesis in the context of whole-cell metabolism.

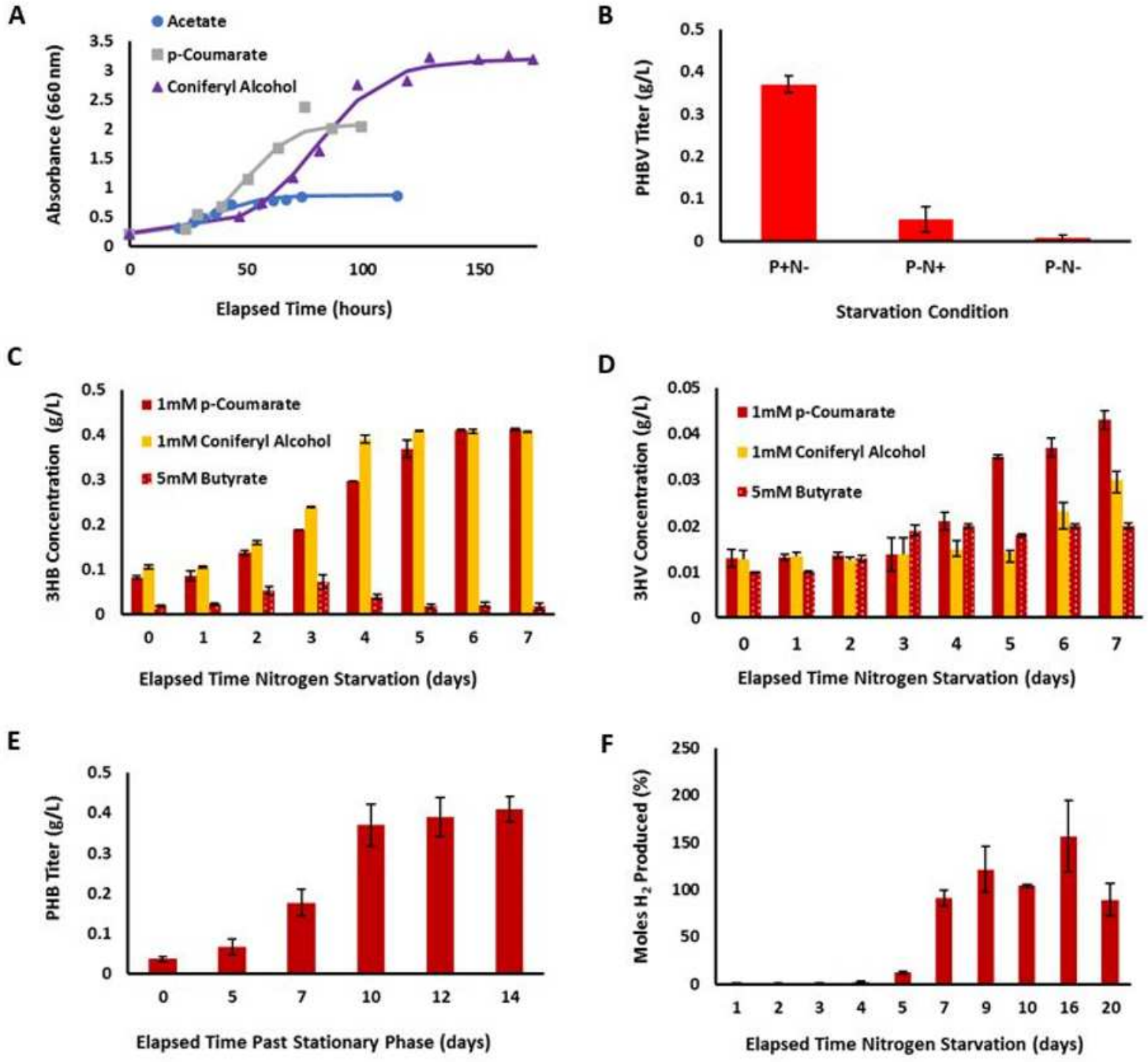

Figure 2

Unique findings from experimental data that motivated application of the GSMM. (A) Anaerobic growth analyses. All substrates were supplemented with 10mM sodium bicarbonate. (B) Starvation condition analysis comparing nitrogen starvation, phosphorous starvation, and a combination of both nitrogen and phosphorus starvation. (C) Comparison of 3HB titers on LBPs vs. butyrate. (D) Comparison of 3HV titers on LBPs vs. butyrate. (E) PHB production from stationary phase (i.e. without resuspending in nitrogen-starved media). (F) Hydrogen production from 1mM p-coumarate after nitrogen starvation. All error bars represent the standard error for the population and are derived from the mean of biological triplicates for each data point.

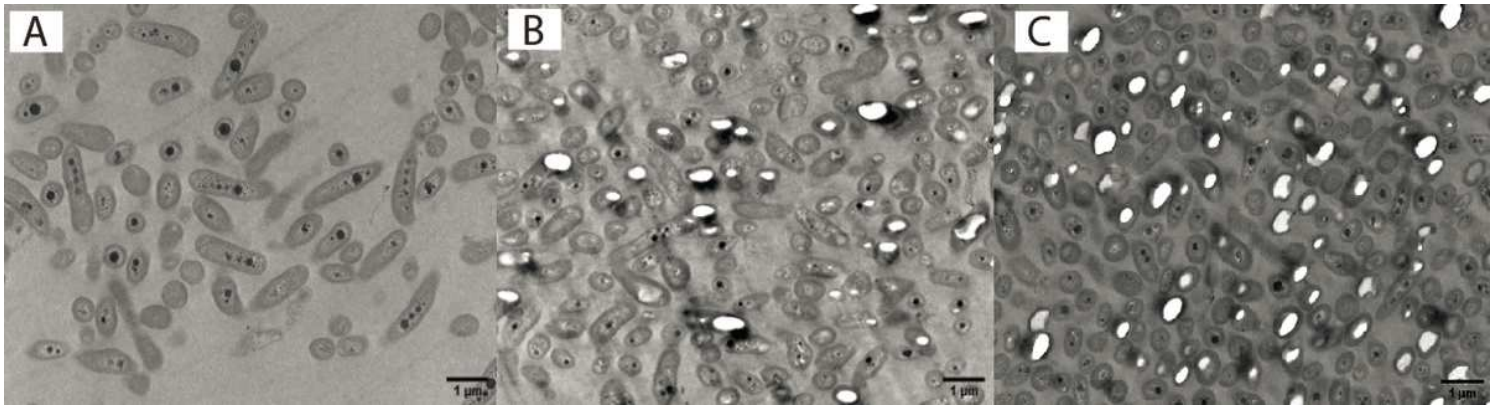

Figure 3

Transmission Electron Microscopy (TEM). TEM images of R. palustris CGA009 cells grown anaerobically in photosynthetic media supplemented with (A) 10mM acetate and 10mM sodium bicarbonate, (B) 1mM p-coumarate and 10mM sodium bicarbonate, and (C) 1mM coniferyl alcohol and 10mM sodium bicarbonate. All samples were grown to mid-exponential phase, and subsequently nitrogen starved for five days. White inclusions inside the cytoplasm denote PHBV granules.

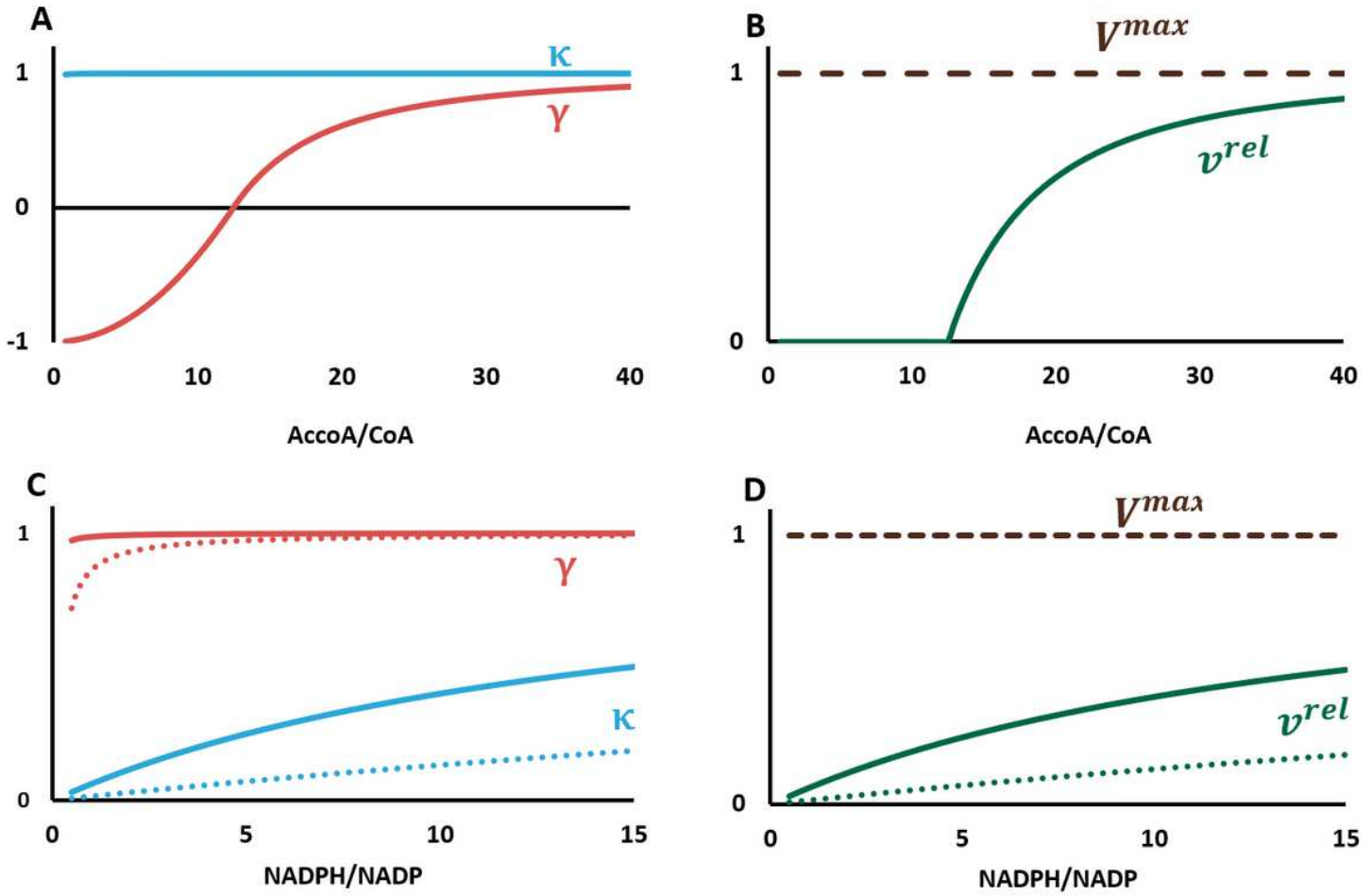

Figure 4

Thermo-kinetic analysis of thiolase (PhaA) and reductase (PhaB) activity. Effect of the acetyl-CoA/CoA ratio on the reaction's (A) thermodynamic driving force (γ) and substrate saturation (κ) and (B) Overall rate relative to Vmax. Effect of the NADPH/NADP ratio on the reaction's (C) thermodynamic driving force (γ) and substrate saturation (κ) and (D) Overall rate relative to Vmax. Solid and dotted lines correspond to a 3-hydroxybutyryl-CoA concentration of 30 μM and 300 μM, respectively.

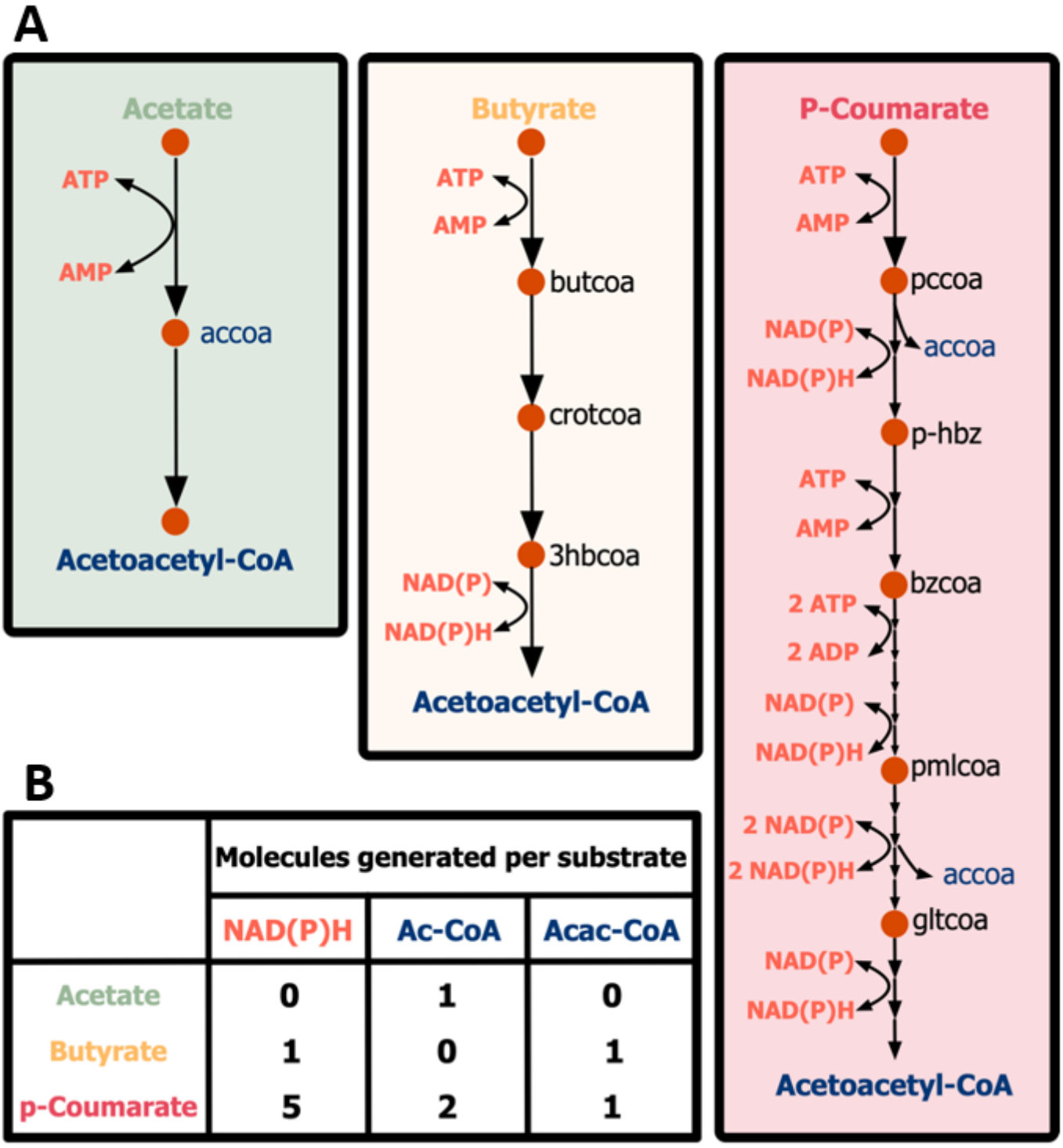

B

	Molecules generated per substrate		
	NAD(P)H	Ac-CoA	Acac-CoA
Acetate	0	1	0
Butyrate	1	0	1
p-Coumarate	5	2	1

Figure 5

Substrate consumption of the three modeled carbon sources: acetate, butyrate, and p-coumarate depicting the (A) breakdown pathways and the (B) relevant cofactors and PHB precursors produced from each carbon source.

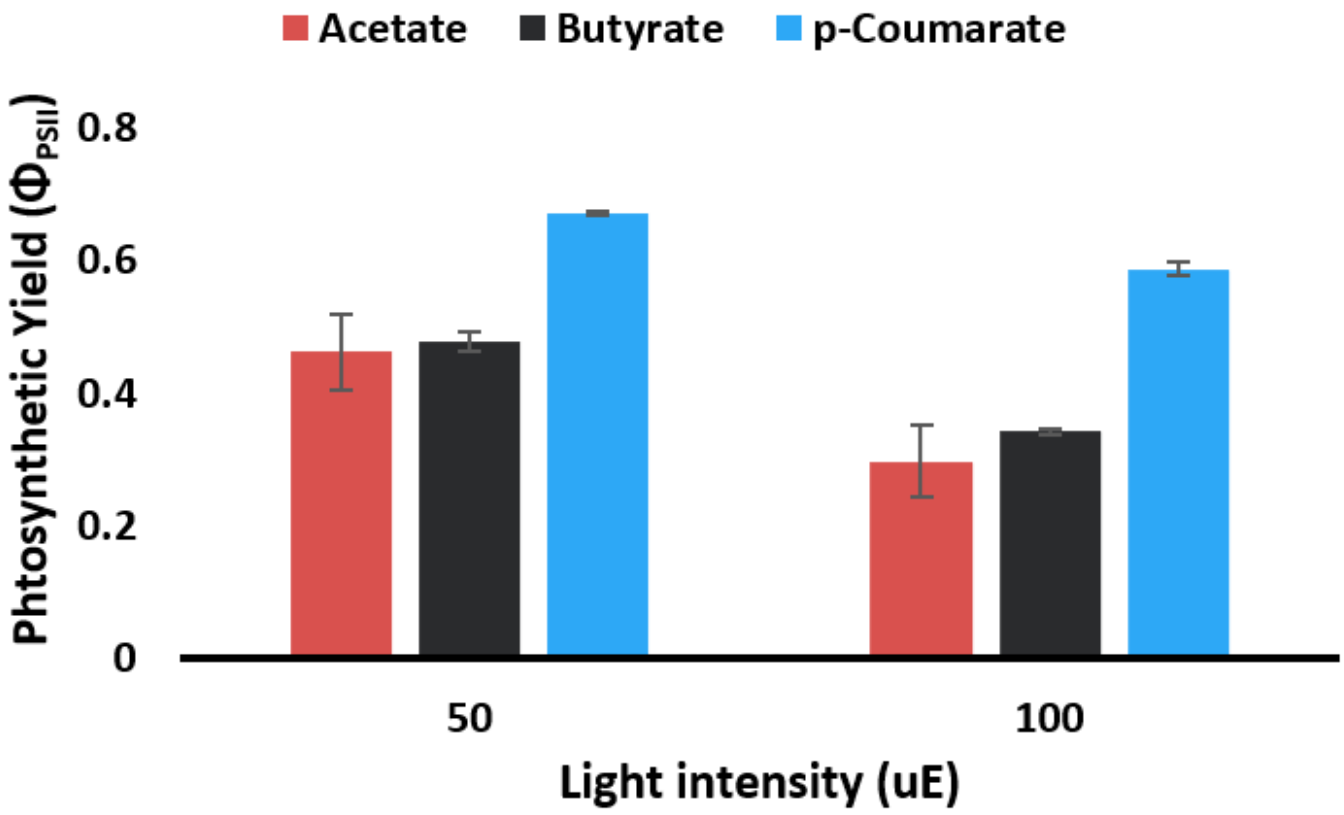

Figure 6

Photosynthetic yields of R. palustris cells grown on different carbon sources as measured at 50 µE and 100 µE.

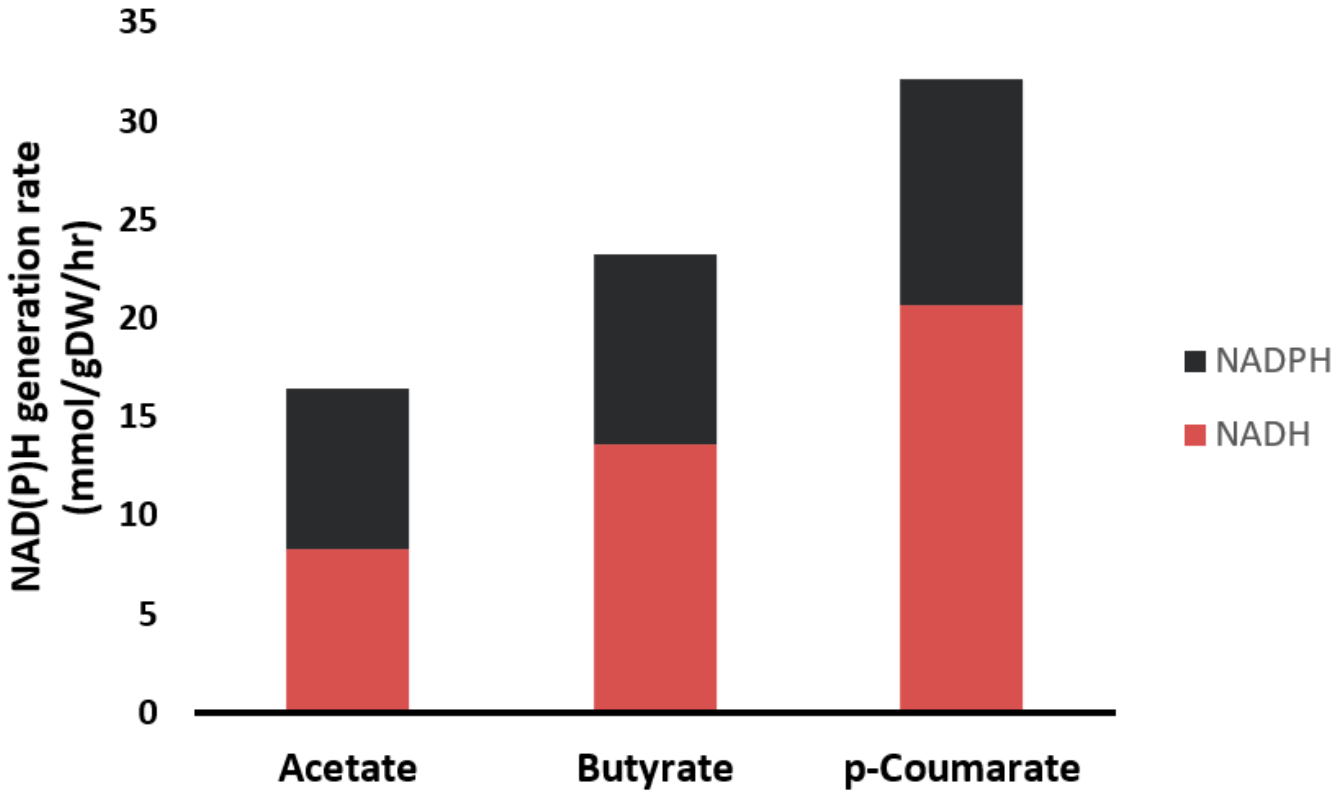

Figure 7

Predicted reduction rates of the cofactors NAD and NADP during growth on acetate, butyrate, and p-coumarate.

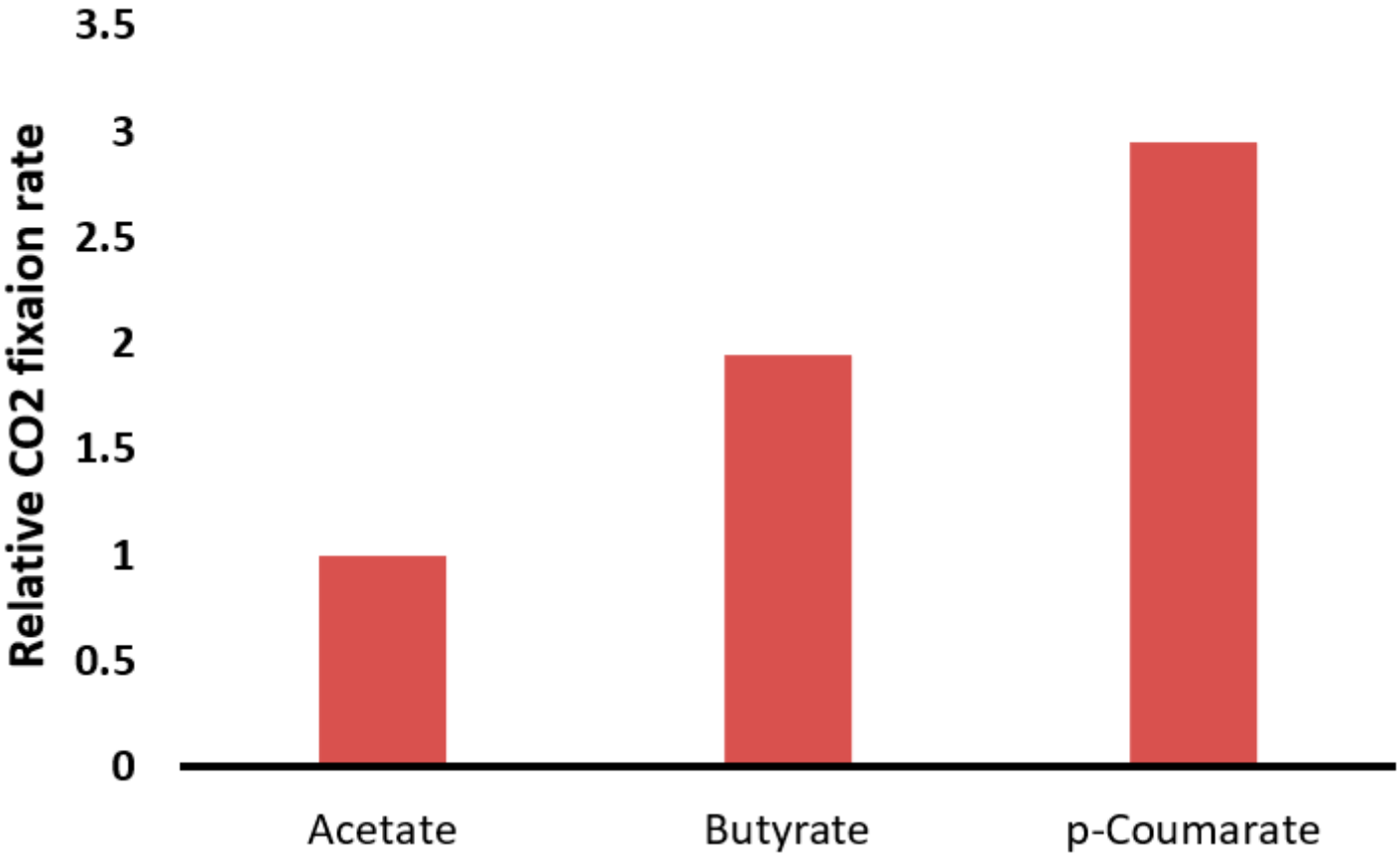

Figure 8

Relative predicted rate of CO2 fixation during growth on acetate, butyrate, and p-coumarate.

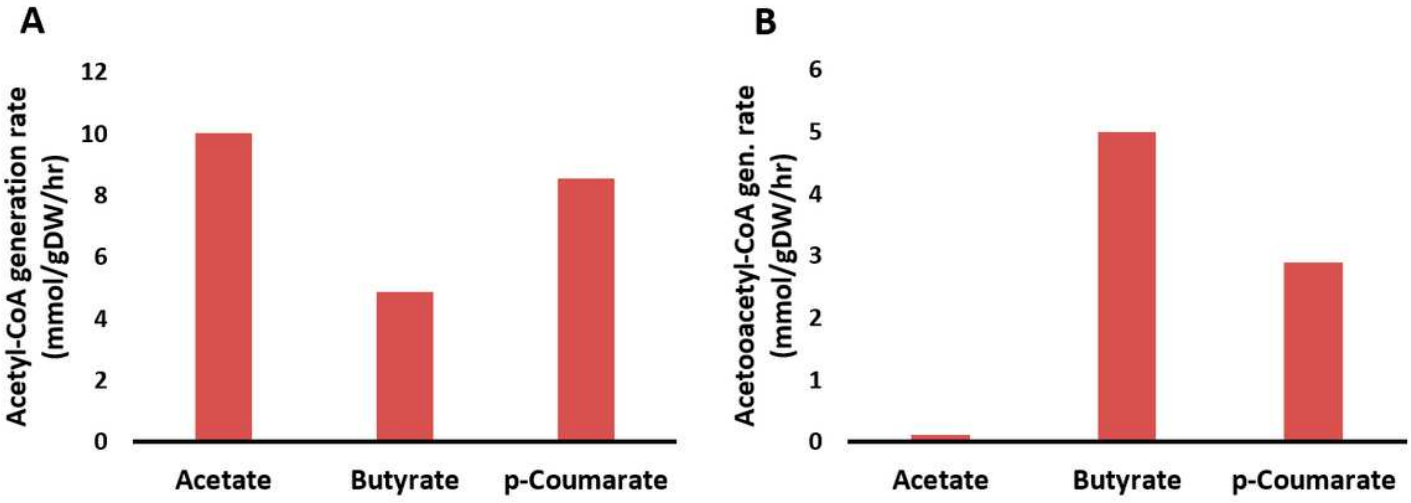

Figure 9

Predicted generation rates of the first two substrates in the PHB pathway (acetyl-CoA (A) and acetoacetyl-CoA (B)) during growth on acetate, butyrate, and p-coumarate.

Supplementary Files

This is a list of supplementary files associated with this preprint. Click to download.

- SupplementaryInformation.pdf